UCL Université catholique de Louvain

École polytechnique de Louvain (EPL)

epl

Characterisation of electric properties in thin bismuth films.

Dissertation presented by
Brice Thomas

for obtaining the Master's degree in
Physical Engineering

Supervisors
Benoit Hackens, Jean-Pierre Raskin

Readers
Vincent Bayot, Thanh Nhan Bui , Sébastien Faniel

Academic year 2017-2018

Acknowledgements

I would like to thank my two supervisors Benoit Hackens and Jean-Pierre Raskin for being present, guiding me in my research and answering my questions, Sébastien Faniel for his implication and helping me in all the experimental aspects of this work. Thann Nhan Bui for providing me his results, his advises and feedbacks on the content of the thesis.

And a special thank to my mother who pushed me through my studies and helped me for proof reading of this work.

Contents

1 Introduction **7**

2 Structure of bismuth for bulk and thin films on Si substrate **8**

2.1 Bulk structure 8

2.2 Thin film structure 8

2.3 Experimental results 11

3 Deposition techniques **15**

3.1 Thermal and electron beam evaporation 15

3.2 Direct and alternating current magnetron sputtering 16

3.3 Pulsed laser evaporation 16

4 Main properties and their physical origin **21**

4.1 Semimetal origin 21

4.2 Classic electronic transport 23

4.2.1 Surface states or correlated conduction channels, two & three-band models . 23

4.2.2 Film Thickness 26

4.2.3 Temperature 29

4.2.4 Size of the grains 35

5 Setup description & Methods **36**

5.1 Objective of the thesis 36

5.2 Components description 36

5.3 Depositions 37

5.4 Configuration description 44

5.4.1 First sample series A 44

5.4.2 First sample series LT, RT & HT 45

5.5 Conductivity acquisition 45

5.6 Calculating bandgap 46

6 Results and Discussion **47**

6.1 Question one: comparison between in situ and ex situ behaviour 47

6.2 Question two: influence of oxidation on conductivity. 49

6.3 Question three: influence of temperature and thickness of film on conductivity . . . 53

6.4 Question four: influence of relaxation of internal constraints on conductivity for freshly deposited films. 57

6.5 Question five: observation of quantum effect in conductivity and comparison with results from literature 58

6.6 Question six: valley of conductivity 61

7 Going further **63**

7.1 Two band model details 67

References **74**

Abreviations

BLs: Bilayers, 1 BL of bismuth = 3.9 Å

HT: High Temperature

RT: Room Temperature

LT: Low Temperature

eV: electron volt 1eV=$1.60217657 \cdot 10^{-19}$ joules

kOe: kilo Oersted, 1 Oe=79.57747 A/m

l_{ϕ}: phase coherence length

SEM: Scanning electron microscope

QSEs: Quantum Size Effects

1 Introduction

The aim of this thesis is to investigate electrical properties of thin bismuth films from 10 to 150 nm thickness deposited on a 90nm SiO_2 layer on top of Si(100). The bismuth has been extensively studied over the last decades as it possesses several unique assets which are described below. This work will carefully examine the conductivity of both in situ and ex situ bismuth films for several thicknesses and temperatures.

- The bismuth is a heavy metal, with a density of 9.78 g cm^{-3}. Its melting point is 271.3 °C or 544,45K [1]. The bismuth is the only metal which is less dense in its solid form than in the liquid state. Just like water, the bismuth expands as it cools.
- The bismuth has a high resistivity (1.29 10^{-6} Ωm at 20°C) and with the exception of mercury, the lowest thermal-conductivity in metals: 7.97$Wm^{-1}K^{-1}$.
- The bismuth also possesses an important magnetoresistance and is the metal with the largest diamagnetic constant of all metals $\chi = -165 \cdot 10^{-6}$ [2]. The temperature and magnetic field applied to the sample will therefore impact its electronic properties[3].
- The bismuth presents a semimetallic/semiconductor transition for thin films[4] [5].

In the scope of this work, we limit ourselves to pure bismuth films and limit the explanation to deposition on Si/SiO_2 substrates.

2 Structure of bismuth for bulk and thin films on Si substrate

Before going further, it is important to understand the bismuth crystal structure and micro/nanostructure for bulk and thin films. Most other properties are influenced by the structure at different scales.

2.1 Bulk structure

The bismuth bulk crystal structure is a A7 rhombohedral unit cell which is presented in Figure 1 and Fig 4 a). Two atoms are contained in this unit cell. The main parameters of this cell are presented below, the experimental values were given by J.L Yarnell et al [6].

- The value of the rhombohedral unit cell primitive vector a_0, which was found to be 4.7236 Å.
- The value of the rhombohedral angle α is 57.35°.
- The position of the second atom. This position is provided by the experimental results $\overline{BD}$= 5.5225 Å and $\overline{DH}$ = 6.2742 Å.

The atom D stands on the trigonal axis, and is nearly at the centre of the cell. However, due to Peierls instability, the atom D is marginally moved along the trigonal axis. This result in three closest neighbours and 3 next-closest neighbours[9]. The bulk bismuth can also be seen has a stack of (1 1 1) atomic bilayers, each bilayer having a thickness of 3.9 Å[10]. L. E. Díaz-Sánchez et al [9] computed the value of the angle between the nearest neighbour atom in a bilayer stack, the angle was found to be 95.63°.

The Brillouin cell of the bismuth is shown in Figure 2. Its structure is similar to the Brillouin zone of a FCC lattice. However, the bismuth has two truly hexagonal faces which are in the trigonal direction (axis z on Figure 2) and the others are "pseudohexagonal".

The electrons are localised in the crystal forming respectively electrons and holes pockets. The hole pockets are located along the trigonal axis [0001] whereas several electrons pockets are present on the "pseudohexagonal" faces. Note that on the picture only 3 of the 6 electron pockets are shown. As the electron and hole pockets are on different symmetry axes, the transport properties will depend on crystal orientation.

2.2 Thin film structure

The thin film microstructure is strongly dependent on deposition parameters. These parameters and deposition technique are later detailed. When a thin film is deposited three cases are possible. The first one is epitaxial deposition, which tries to deposit a perfect match between the substrate and the crystal. This is intend to produce a crystal close to the bulk material. Another case is the random deposition. The resulting film has no preferred orientations. The last case which is the most common is the textured deposition. In that case, the deposition is not epitaxial, but several crystal

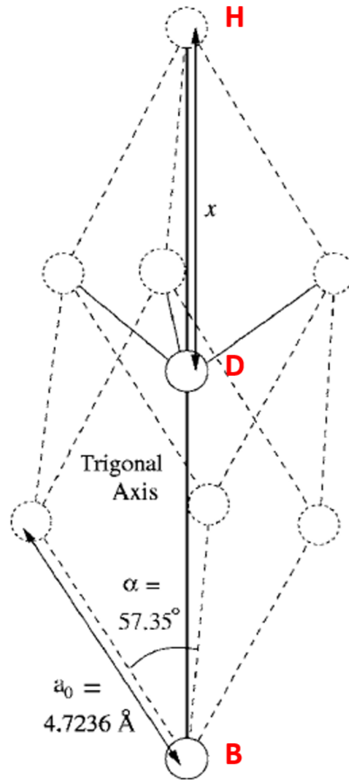

Figure 1: Bulk bismuth atomic structure with experimental lattice parameters. The bold line marks the trigonal axis, the dashed lines mark out the unit cell, while the remaining solid lines indicate the bonding. The two atoms in a primitive unit cell are shown as solid circles, while adjacent atoms are dashed [7].

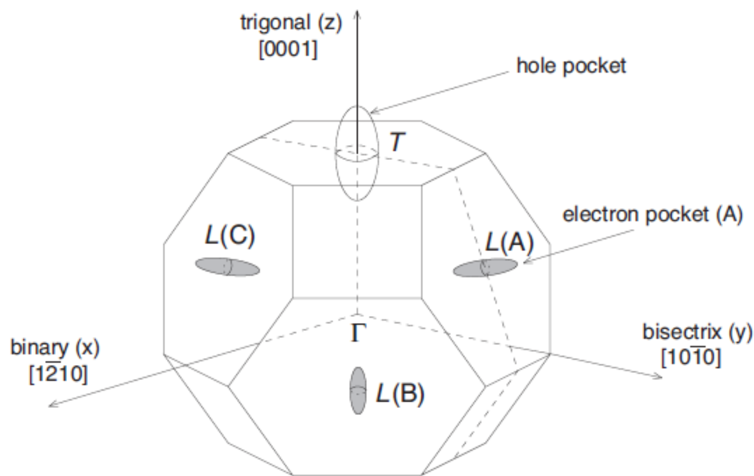

Figure 2: The Brillouin zone of Bi, with the Fermi surfaces of electron pockets at L-points (shaded areas; only 3 among 6 are shown) and the hole pocket at T-point [8]

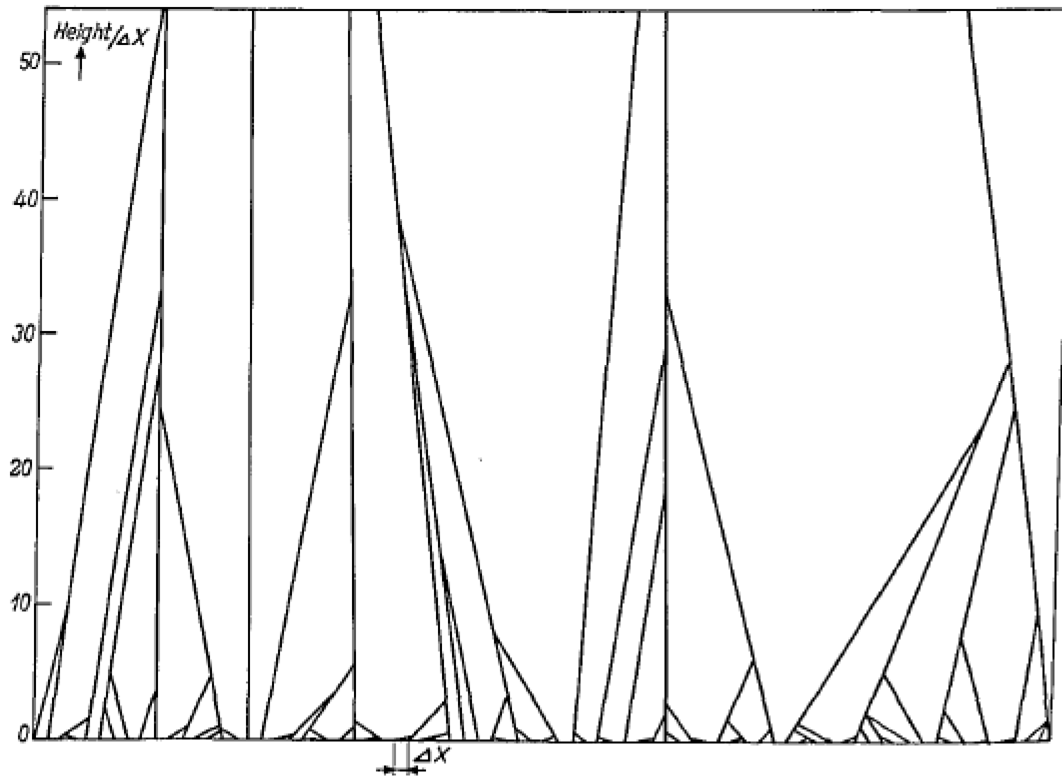

Figure 3: The evolutionary selection during growth starting from randomly orientated equidistant nuclei on a one-dimensional substrate (bottom line) in a two-dimensional space, is shown. The assumption is that the vertical component of the growth rate is larger at steeper orientations of the crystal. The height above the substrate is expressed in the unit Δx, the distance between two nuclei [11].

orientations tend to dominate the film's structure.
Thin films of bismuth on silicon substrate at room temperature, tend to form hexahedron-like structure Fig 4a) and to make them grow until they coalesce with each other and create a continuous film. The grains are the result of these growing hexahedrons.

When the bismuth is deposited on a silicon substrate by a vapour deposition method, it creates small nuclei. These nuclei start with random orientations. As the deposition proceeds, all these random orientated grains start to grow. What is really important to understand, is that all those directions do not grow at the same rate. Some of them grow much faster than the others. When these grains grow, they will end up meeting each other, as A. Van der Drif [11] explained, only the fastest growth directions will survive. When two growing grains meet, only the one which has already grown the steepest one compare to the substrate will continue to grow, and the other one will stop. This concept is illustrated in Figure 3, where it is clear only the few fastest growing directions will remain. This explains why in thin films, several growing directions are observed. These directions depend on the material deposited, the substrate and the deposition conditions which affect the crystal's growth rate.

The film has thus three different stages, the first one is the nucleation where all the crystals are randomly oriented. This film has a high roughness because fast and slow nucleation, growth are present, and the entire substrate is not coated yet. Afterwards, a critical thickness is reached where the roughness is minimal. At this point, the film is entirely coated, and the grains tend to be roughly the same height and width. Once the thickness is passed, the crystal will become rougher again, several grains will continue to grow quickly, whereas other regions will have slow or no grain growth. The roughness will thus continue to increase with the thickness of the film. Those fast-growing crystals are called Hillocks.

2.3 Experimental results

Experimental results for thin film must be separated into two categories. Epitaxial depositions which should provide a result close to the bulk structure. Non-epitaxial deposition, give rise to Hillocks and the roughness of the film, whereas epitaxial is indented to produce a perfect crystal. An illustration of the cell of the bismuth structure with a clear depiction of the Rhombohedra structure is illustrated on Figure 4 [12]. This is the result of an epitaxial deposition of Bi (111) on a $NbSe_2$ substrate at 350K.

For non-epitaxial deposition, we can look at the work of Y. Ahn et al[13] who deposited bismuth thin films on (100) silicon. In this work, the bismuth was deposited at room temperature on silicon substrate under a 10^{-8} torr vacuum by molecular beam deposition using Knudsen-cell (K-cell). The thickness of the films ranged from 7 to 66.6 nm.

The film deposited clearly exhibits the three stages explained in subsection 2.2. The bismuth deposited by vapour covered the substrate by creating grains with random orientation and voids between them. The voids then tend to disappear as the grains meet to form a uniform film. This coalescence occurs here around 13 to 18 nm as it can be deduced by the measure of the electric coalescence, Figure 5a and the root mean roughness measure, Figure 5b. After this thickness is passed, the film starts to get rougher again. The roughness of the film continues to increase as the size of the film increase. This is due to the fast-growing directions which create Hillocks. AFM pictures of the sample are presented in Figure 6. Now that the three main stages are explained, we will focus on the structure of bismuth. When the coalescence occurs between the different grains, elongated grains are created. These elongated grains can be seen by comparing Figure 6 a) and b). Even though the grains are elongated, voids are still present between them. As the deposition carries on, the void will be filled, and the film will be smoother. As the film thickness reaches 18 nm, the grains on the surface start to exhibit polyhedral shape. By observing Figure 6, it is clear that thin and thicker films do not have the same topography. For thinner films, all the grains are about the same height and width. Whereas, for the thicker films, some grains can have a 50 nm height and 100 nm width and other only 10 nm height but 200 nm width. Another consequence of the coalescence and the holes-filled up, is that the density of the film increase with the thickness until reaching bulk density. For the films of thickness 9.3 and 12.4 nm, their densities are 4.985 g/cm^3 and 7.918 g/cm^3. The first one is half of the bulk density, which is 9.78 g/cm^3. On the other hand, the 18 nm film has this bulk density. This means that the film undergoes an important surface microstructure evolution between 13 and 18 nm. The increased density is the result of the holes getting filled by the additional matter.

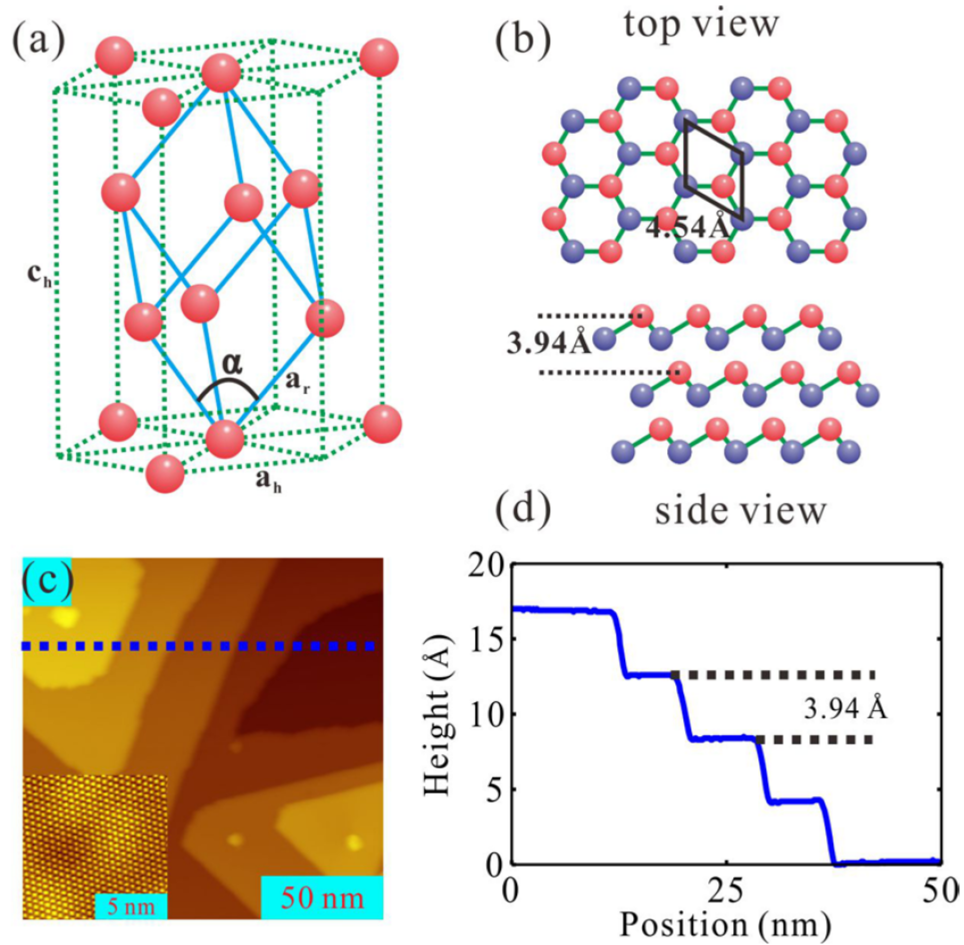

Figure 4: Crystal structure of bulk Bi and epitaxial Bi(111) on $NbSe_2$. (a) Rhombohedra structure (blue solid line) and hexagonal structure (green dashed line) of Bi. (b) Crystal structure of Bi(111) surface. Top layer atoms (red spheres) and bottom layer atoms (blue spheres) form a buckled honeycomb structure. (c) STM image of Bi(111) on $NbSe_2$. Inset: Atomic resolution image taken from the surface in (c). (d) Line profile taken from the dashed (blue) line in (c). The STM image was taken with tunnelling current I = 0.1 nA and STM bias V = 1.0 V. Atomic resolution image was taken with I = 0.2 nA and V = 100 mV.[12]

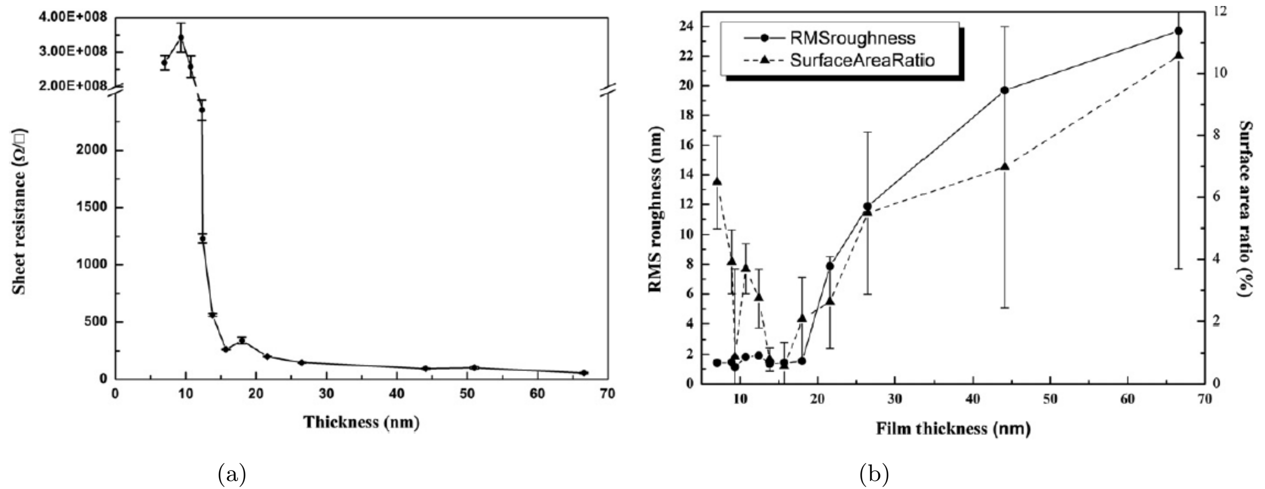

(a) (b)

Figure 5: (a) Change of sheet resistance as a function of bismuth film thickness. Numerous investigations are conducted, and standard deviations shows as error bars [13]. Samples are bismuth films deposited on silicon (100) substrates at room temperature. (b) RMS roughness and surface area ratio (SAR) as a function of the film thickness [13]. Samples are bismuth film deposited on silicon (100) substrates at room temperature.

Now that the surface densities and growth have been explained, it is important to mention that growth directions have also been altered during the growth. This can be seen in Figure 7. The peaks are in the (003) and (006) directions (in the hexagonal crystallographic system). A slight peak is also present in the (009) direction but was not shown on the figure because the dominant silicon (001) crystal peak. It is clear that the apparition of the peaks on this figure coincide with the surface transition mentioned earlier.

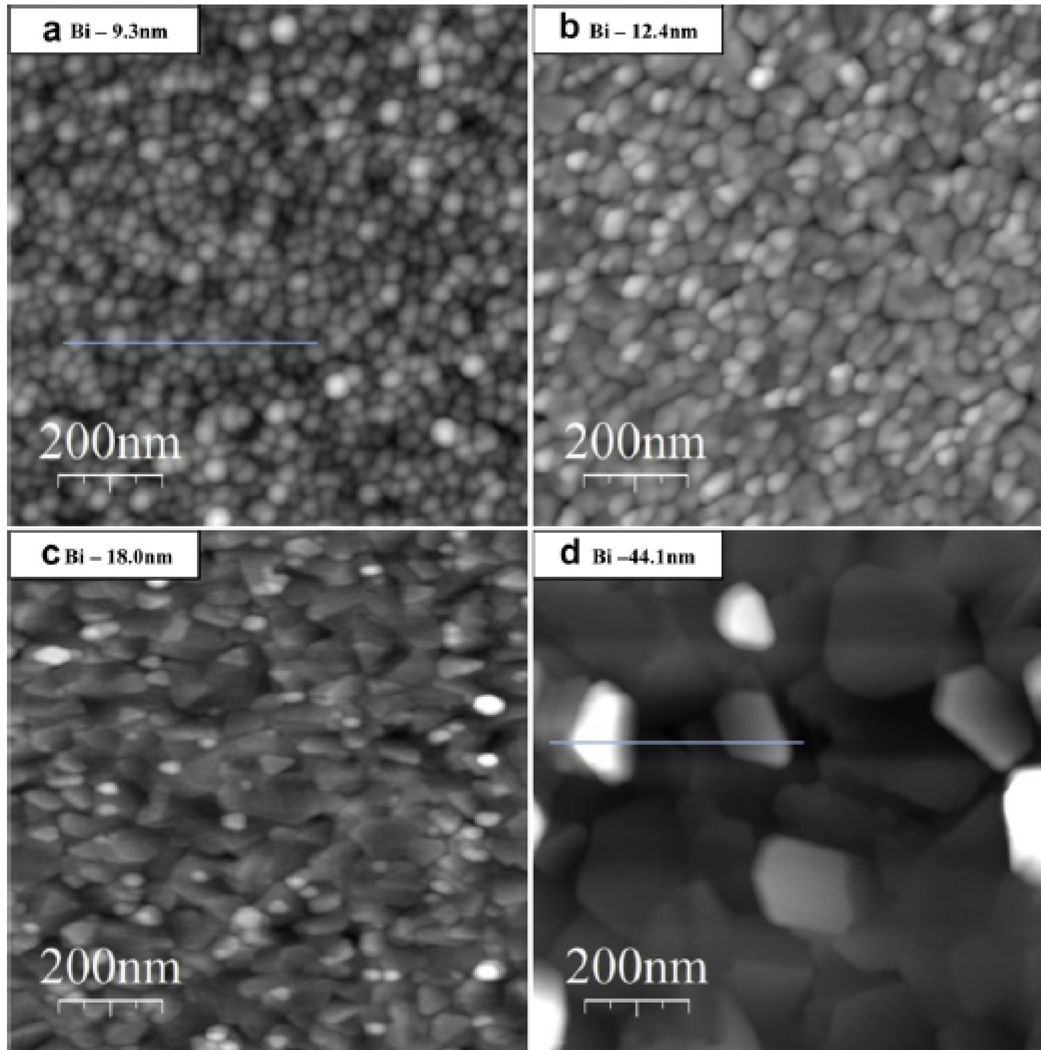

Figure 6: bismuth films deposited at Room Temperature on (100) silicon by molecular beam deposition. Atomic force microscopy (AFM) images and cross sectional profiles of bismuth thin films. (a), (b), (c), and (d) show the surface morphology of the film with 9.3 nm, 12.4 nm, 18.0 nm, and 44.1 nm thickness, respectively.

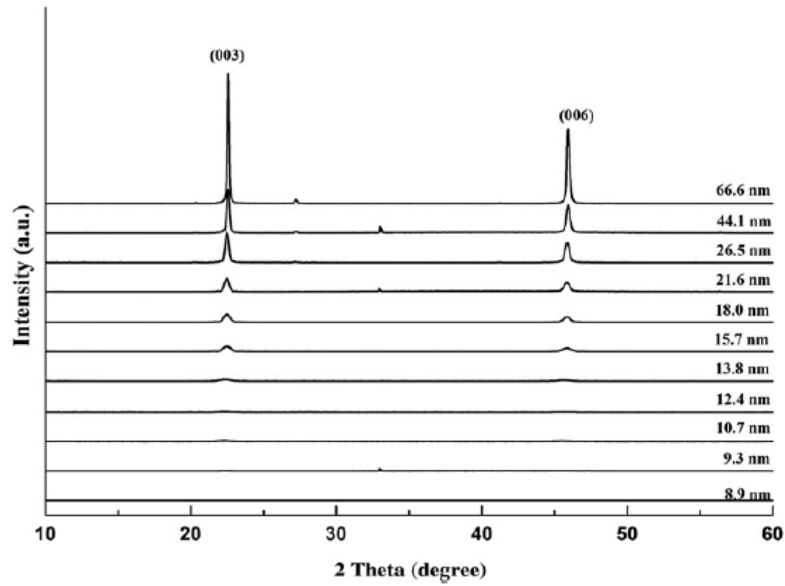

Figure 7: X-ray diffraction (XRD) patterns for various bismuth film thickness.

3 Deposition techniques

Several deposition techniques are currently used to create bismuth thin films. In this section we discuss what are their differences and their respective advantages.

The deposition techniques described are the following:

- Thermal and electron beam evaporation
- Direct and alternating current magnetron sputtering
- Pulsed laser evaporation

The vapour phase of the bismuth is used in all those different methods. However, they differ by the energies associated with the impinging species [14]. Bismuth grows in a textured crystalline microstructure which means that a relation exists between the substrate axis and the axis of the growing bismuth.

3.1 Thermal and electron beam evaporation

The deposition with the lowest energetic deposition is the evaporation. The energy received while being deposited is in the range of 0.1-0.25 eV. On silicon substrates, this favoured the (003) orientation in the hexagonal crystallographic system. Or, in other words, the trigonal axis is perpendicular

to the substrate plane. The substrate is usually not heated during an evaporation. Thermal evaporation favours large grains in the film on silicon substrates. [13]. Figure 8 illustrates the results obtained by S.E. Rodil et al. Figure 9 specifies the deposition conditions for evaporated samples.

3.2 Direct and alternating current magnetron sputtering

Magnetron sputtering usually provides energy in the range from 0 to 25 eV [15]. Depending on the pressure and plasma conditions the particles are deposited on the substrate at energies in the range of 0.1 to 5 eV. Experiments tend to show that for low thicknesses (below 200 nm) on a silicon substrate, the (003) is favoured and afterwards several peaks appear in the (012), (003) and (104) directions. The substrate tends to be in a temperature range of 150-250 °C. This influences the microstructure. Figure 10 & 12 illustrate the results obtained by S.E. Rodil et al. Figures 11 & 13 specify respectively the deposition conditions for DC-sputtered and RF-sputtered samples.

3.3 Pulsed laser evaporation

In Pulsed Laser Deposition (PLD), most of the particles arrived as charged ions. The energy range of those ions is between 100 and 300 eV. This results in an energetically driven growth and not a thermodynamic one as from the evaporation of sputtering. However, the film still grows in the (003) direction independently of the thickness. At higher energies, the (012) direction is preferred. Figure 14 illustrates the results obtained by S.E. Rodil et al. Figure 15 specifies the deposition conditions for pulsed laser deposited samples.

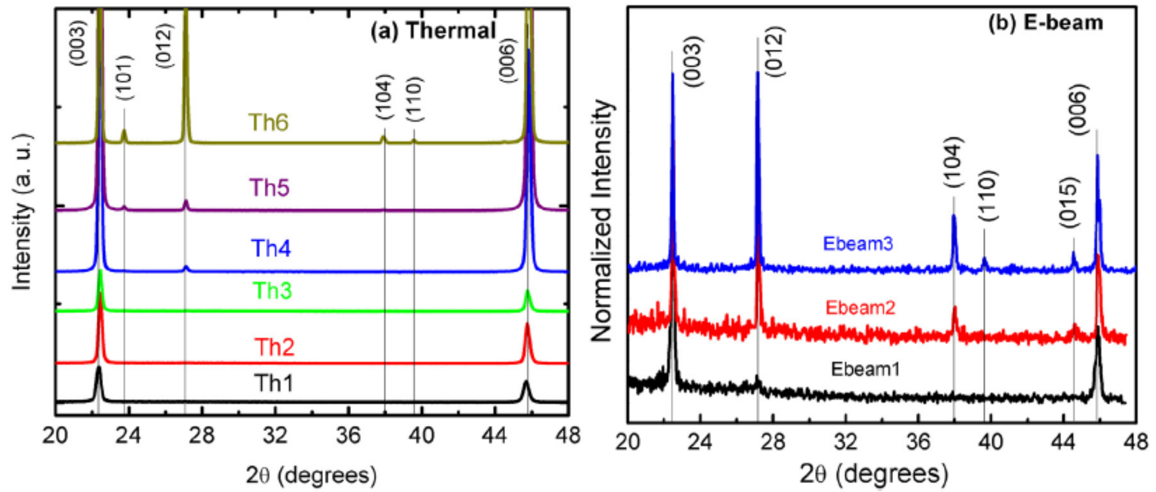

Figure 8: X ray-diffraction patterns of the Bi thin films deposited by evaporation (a) Thermal evaporation as a function of the deposition time; the patterns were not normalized and (b) E-beam evaporation as a function of the source-substrate distance. [14]. a) Thermal deposition on glass substrate was not heated vacuum was 10^{-3} Pa. b) E-beam deposition with a distance of 75, 25 and 12 cm and an exposition time of 100s. Resulting in respectively: 180,500 and 850nm film thickness.

Sample name	Time (s)	Distance (cm)	Thickness (nm) $\pm 5\%$
Th1	5	3	71
Th2	15	3	75
Th3	25	3	150
Th4	40	3	287
Th5	80	3	474
Th6	180	3	2029
Ebeam1	100	75	180
Ebeam2	100	25	500
Ebeam3	100	12	850

Figure 9: Deposition conditions and thickness of the samples deposited by evaporation in Figure 8 [14].

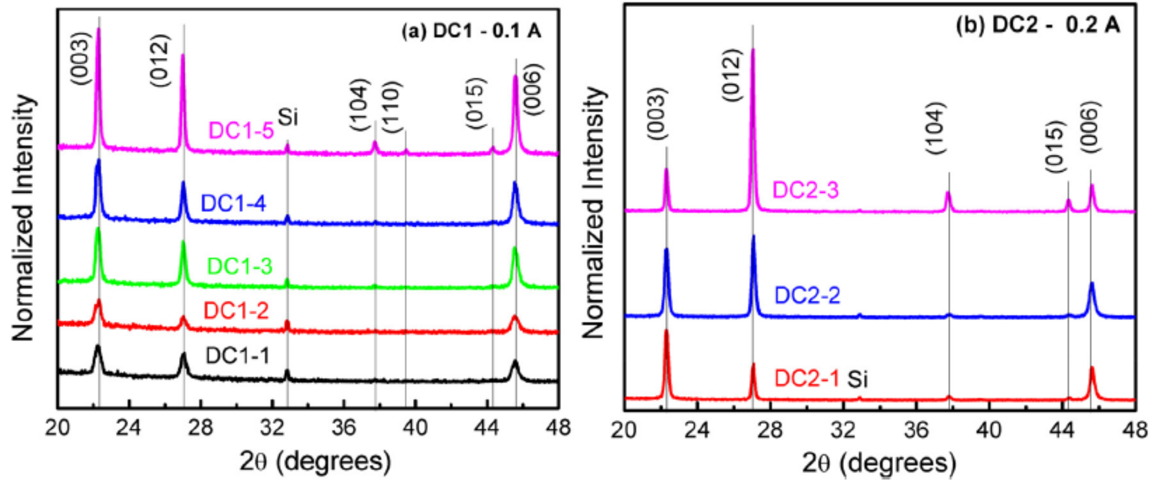

Figure 10: X-ray diffraction patterns of the Bi thin films deposited by DC magnetron sputtering. Base pressure $6*10^{-4}$ Pa and 4 Pa of working pressure. Thickness from 170 to 2262 nm. Deposition on silicon (100) and glass. Base pressure $1.4*10^{-4}$ Pa and 4 working pressure of 4 Pa. Thicknesses from 10 to 1400 nm. [14]

Sample name	Current (A)	Time (s)	Thickness (nm) ±5%
DC1-1	0.1	30	12
DC1-2	0.1	50	27
DC1-3	0.1	70	57
DC1-4	0.1	90	62
DC1-5	0.1	300	186
DC2-1	0.2	50	118
DC2-2	0.2	90	173
DC2-3	0.2	300	449
DC2-4	0.2	600	1394

Figure 11: Deposition conditions and thickness of the samples deposited by DC-sputtering in Figure 10 [14].

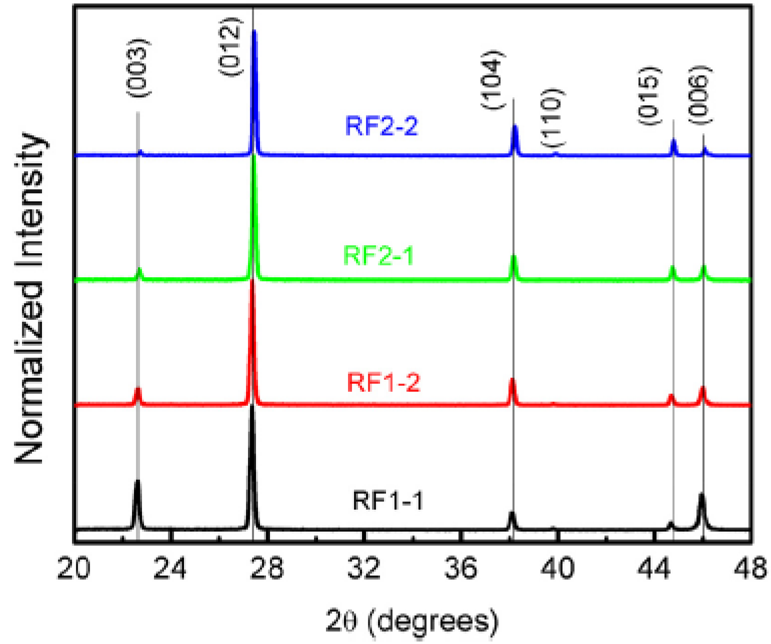

Figure 12: X-ray diffraction patterns of the samples deposited using RF magnetron sputtering.[14]

Sample name	RF power (W)	Time (s)	Thickness (nm) $\pm 5\%$
RF1-1	45	300	604
RF1-2	45	600	1200
RF2-1	60	600	170
RF2-2	60	900	2262

Figure 13: Deposition conditions and thickness of the samples deposited by RF-sputtering in Figure 12 [14].

S.E. Rodil et al. / Thin Solid Films 636 (2017) 384–391

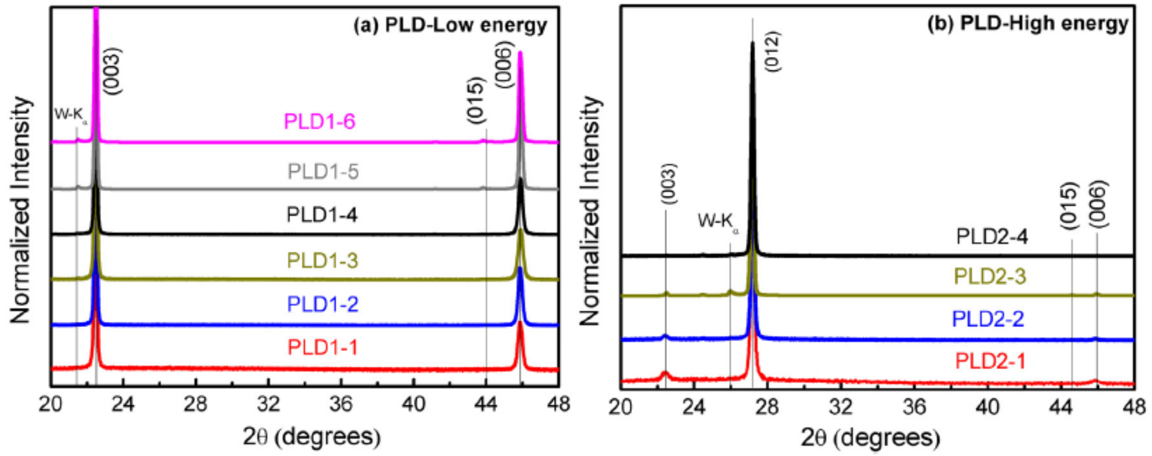

Figure 14: X-ray diffraction patterns of the Bi thin films deposited by pulsed laser ablation using (a) low ionic energy (110 eV) and (b) high ionic energy (270 eV). [14]

Sample name	Bi ion energy (eV) ±10 eV	Deposition time (min)	Thickness (nm) ±5%
PLD1-1	120	4	20
PLD1-2	100	15	54
PLD1-3	103	20	110
PLD1-4	118	30	150
PLD1-5	113	40	200
PLD1-6	110	60	600
PLD2-1	260	15	60
PLD2-2	270	25	100
PLD2-3	280	40	200
PLD2-4	270	60	800

Figure 15: Deposition conditions and thickness of the samples deposited by pulsed laser deposition in Figure 14 [14].

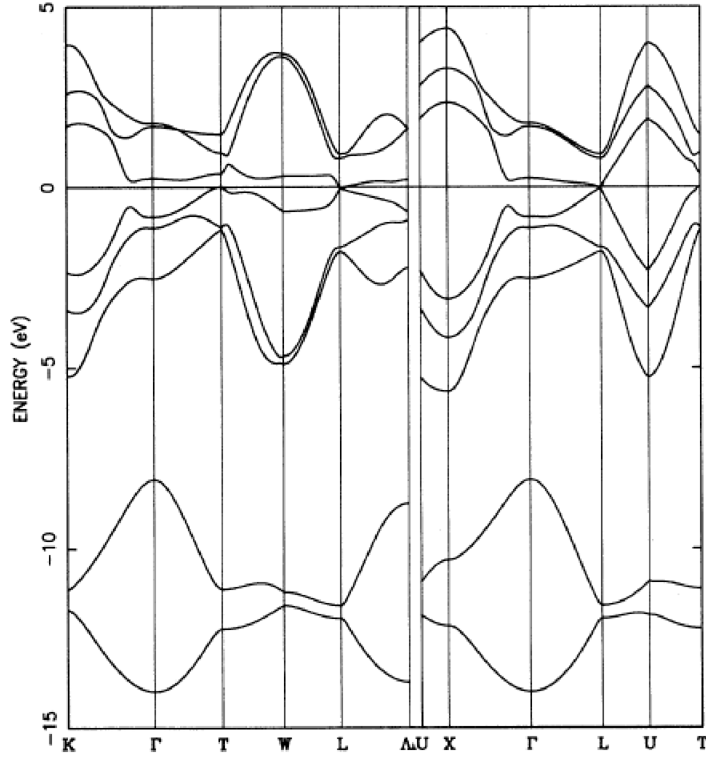

Figure 16: Band structure of Bi along various symmetry lines[16].

4 Main properties and their physical origin

4.1 Semimetal origin

Bismuth is a semimetal which presents a semimetal/semiconductor transition. Semimetals have a band structure depicted in Figure 17 a) in which a conduction and valence band overlaps [16]. The bismuth has a weak overlap which means that it only possesses a small number of free electrons and holes. It is clear on Figure 17 that the L electron band start to be filled with electrons before the holes band is filled. The bismuth band structure is given in Figure 16. Density of states of bismuth at the Fermi level is negligible[14]. This is one of the reasons why it is not a good conductor.

The bismuth has a small energy gap between valence and conduction bands. The resulting properties of this band structure are: high carrier mobilities, small effective masses, large electron mean-free path and long Fermi wavelength ($\lambda_F \approx 30$ nm) [18].
The effective masses of bismuth are strongly anisotropic, one of the consequences is the distribution of electrons and holes in several pockets in the Brillouin cell. The effective masses of electrons and holes have been computed by Y. Liu et al [16]. By rotating the system by a tilt angle of 6° being the rotation between the crystallographic reference frame and the electron ellipsoid axes. The ef-

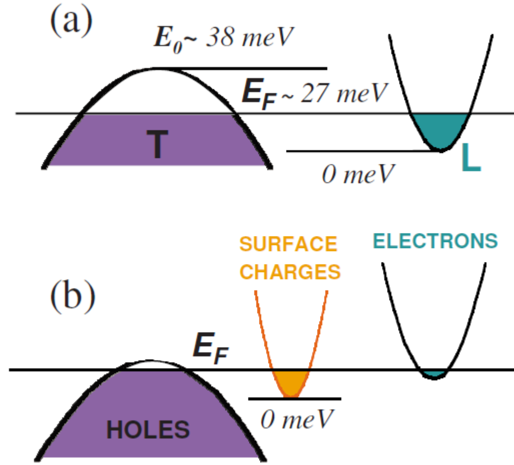

Figure 17: (Colour online) Schematic energy-band diagram showing the energies of the band edges for the L-point electron pockets and the T-point holes and the Fermi level for (a) bulk Bi, where the band overlaps is 38 meV and Fermi level is 27 meV from the bottom of the L-point pocket band edge, and (b) tentative energy-band scheme for ultrathin Bi films [17].

fective masses are m_1=0.198 (m_e), m_2=0.00147 and m_3=0.00215 for the electrons and m_1=0.0675, m_2=0.0675 and m_3=0.612 for the holes. The bismuth has an indirect negative bandgap, this is due to the conduction-band minima (at L point) being 38 meV under the valence band maxima (at T point).

A semiconductor possesses a gap between its conductance and valence band. This gap makes the semiconductor transport thermally activated. Carriers will be generated as the temperature increases. Conversely, when the temperature decreases, the number of carriers is diminished and thus the resistivity increases. If a gap is present, the resistance of the semiconductor will increase as the temperature drops. But resistance can still increase as the temperature drops without necessarily the presence of a gap. A transition from semimetal state to semiconductor happens when the lowest electron subband rise above the highest hole subband. C.A. Hoffman et al reported one of the first observation of this transition in bismuth [4]. This paper created a debate within the scientific community. Computation predicted this transition, but the experimental confirmation took some time to be achieved. In C.A. Hoffman et al work, they produced Bi films with thickness of 200, 300, 400 and 5000 Å. The films were put in a heterostructure of CdTe by epitaxial deposition. They experimentally measured a difference of behaviour between the 300-5000 Å films and the 200 Å one. This difference can be seen in Figure 18a & 18b. To do so, they made the following reasoning on Figure 18b: for the 300-400 Å film, the n(T) dependence indicated strong thermal activation. As temperature reached 300 K, p/n rapidly approached unity showing the perfect compensation that was expected. Moreover, p and n approached the value of the 5000 Å film. In the 200 Å film, it was not possible to detect electrons until the temperature reached 200K. At 300K, the electron density in the 200 Å film, was still 5 times lower than n in the other films, even though the hole concentration was approximately equal for all films at that temperature. These results suggested that the conduction band was at a minimum and the valence band was at a maximum, both being separated by an energy gap. By looking the intrinsic carrier concentration as function of

the temperature, they could figure experimentally that the 200 Å film possessed a 40 meV bandgap and thus had a semiconductor behaviour. The complete investigation can be found in reference [4].

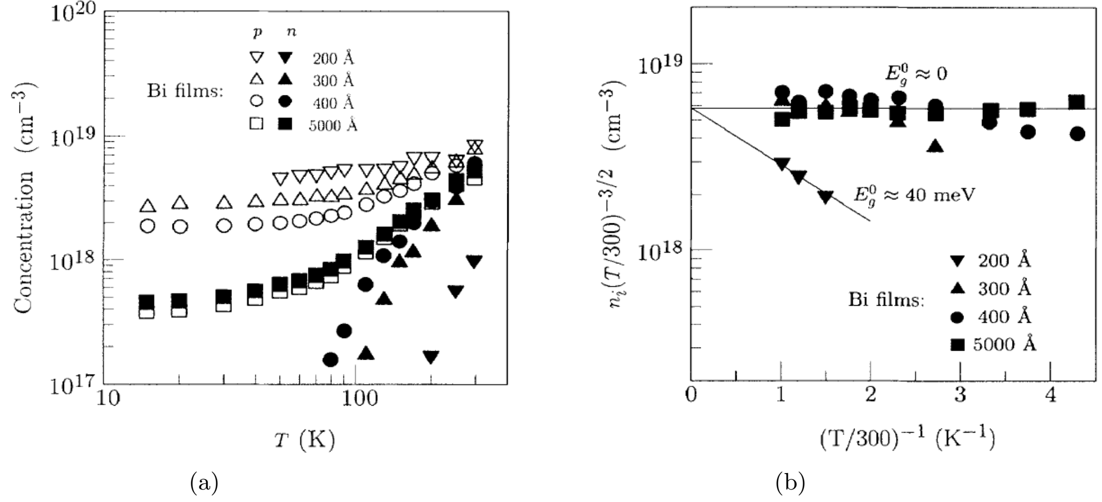

Figure 18: (a) Experimental electron and hole concentrations vs temperature in four Bi films with thicknesses between 200 and 5000 Å. (b) Intrinsic carrier concentration (normalized to $T^{3/2}$) vs inverse temperature in four Bi films with thicknesses between 200 and 5000 A. [4].

4.2 Classic electronic transport

Several factors influence the transport properties in thin bismuth films on silicon substrates. We will now list them and detail their influence. These factors are:

- The surface states
- The film thickness
- The temperature
- The size of grains
- The magnetic field[1]

4.2.1 Surface states or correlated conduction channels, two & three-band models

Even though surface states are not a true adjustable parameter and are not something that scientist can control unlike film thickness, temperature or magnetic field, the surface states play a great role

[1]The magnetic field will not be treated in this thesis as no experimental results implying magnetic field are presented.

in thin film transport in particular in the case of bismuth. As the other parameters will refer to surface state conduction, we think that it is important to explain what are surface states.

As the thickness shrinks, bulk contribution to the electrical transport is not anymore the only contribution which is observed [17]. A contribution due to the surface is present, this conductivity is called surface conductivity and is a result of surface accepting states. When the thickness of the film diminishes, the bulk contribution is decreased, therefore the surface states become gradually more important. This surface states contribution can be accounted for the transport properties of film of about 20-30 nm thickness and below[17]. Conversely, bulk contribution can be neglected for these thicknesses. On the other hand, for thick films as 100 nm and above, the contribution of surface states is negligible compared to the bulk transport. Therefore, they can be neglected. This is one assumption that will be used to interpret our results. It is based on Equation 6.6 in Section from Xiao et al [19].

These surface states possess an energy level in the gap between the conduction and valence bands. An illustration of these surface states is given in Figure 17b).

Bismuth exhibits an electrical conduction (σ_{xx}) which is thus the sum of two contributions. The first contribution is the contribution of the surface S (σ_s) which is assumed to be independent of the thickness and the second being the bulk conduction in the film[19].

$$\sigma_{xx} = \sigma_S + \alpha \cdot e^{-(\frac{\Delta E_g}{2kT})} \tag{1}$$

We define a constant b such as $\Delta E_g = \frac{2b}{d^2}$. The conductivity can thus be rewritten as:

$$\sigma_{xx} = \sigma_S + \alpha \cdot e^{-(\frac{b}{kTd^2})} \tag{2}$$

This expression contains now only two parameters which are the thickness of the film and the temperature. These two parameters will be modified in the different depositions in order to extract the band-gaps in the films.

To provide the charge carrier densities as well as the mobilities in bismuth films a two-band model is used. This model is explained by N. Marcano et al [20] and is used to analyze 300 nm thick bismuth samples .

This band model is based on the conduction of electrons and holes in the film. As two different types of carriers are present, it is called a two-band model. Each band as its own resistivity(ρ_1, ρ_2) and its Hall resistivity $\rho_{Hall,1}, \rho_{Hall,2}$. To extract the carriers, they fit the magnetoresistance and Hall resistance both as a function of the temperature and applied field. The equations are given as follows by equations 3 & 4. Further information on this model is present in the annex 7.1.

$$\rho_{Hall} = \frac{R_e R_h (R_e + R_h) B^3 + (R_e \rho_h^2 + R_h \rho_e^2) B}{(\rho_h + \rho_e)^2 + (R_h + R_e)^2 B^2} \tag{3}$$

$$\rho = \frac{\rho_e \rho_h (\rho_e + \rho_h) + (\rho_e R_h^2 + \rho_h R_e^2) B^2}{(\rho_e + \rho_h)^2 + (R_e + R_h)^2 B^2} \tag{4}$$

with $\rho_e(\rho_h)$ as the resistivity and $R_e(R_h)$= -1/qn (1/qp), the Hall coefficient for the electron (hole) band and B being the applied magnetic field [20].

This two-band model states that the Hall resistivity is in most cases not linear with the magnetic field. This non-linearity suggests the non-compensation of the two carriers (electrons and holes) in these thin films. Equation 4 enables to extract the carrier density ratio (p/n) as a function of temperature. Figure 19a & 19b shows the Hall resistivity and carrier concentration as a function of temperature that were obtained by N.Marcano et al[20]. At high temperatures, the carrier concentration of electrons is higher than for holes: $(n/p > 1)$. For temperature lower than approximately 100K, the conduction by holes dominate, resulting in $(n/p < 1)$.

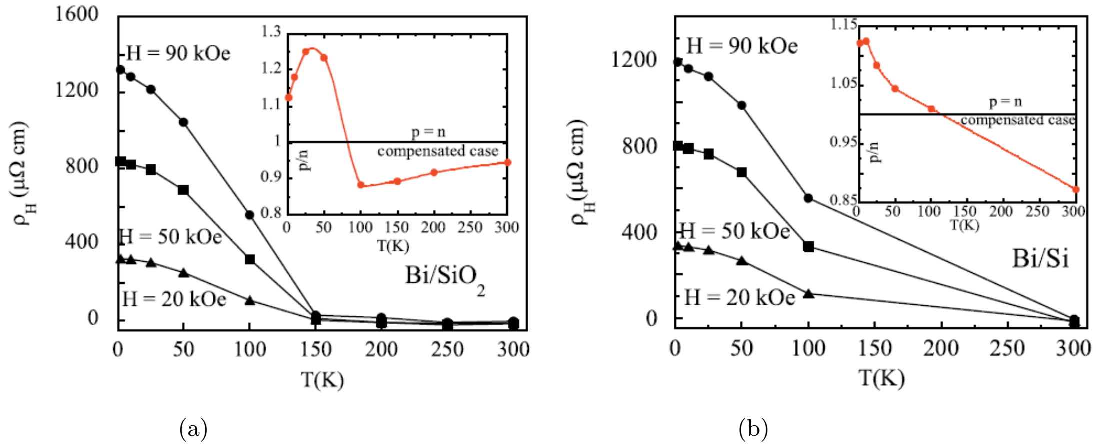

(a)

(b)

Figure 19: Hall resistivity at 20, 50 and 90 kOe as a function of Samples A and B. The inset shows the density carrier ratio (n/p) obtained from fits to Equation 4. 300 nm thick Bi film on Si (001) using a buffer of 800-nm-thick deposited by thermal evaporation of (a) SiO_2. (b) highly resistive Si [20].

This paper was focused on 300 nm thick films. In that case a two-band model is enough. But for the thicknesses of approximately 20-30 nm or lower, a three-band model taking into account the surface states conduction is required.

As mentioned before, bulk bismuth exhibits n-type conductivity. However, in the studies of thin film, it is mostly p-type electric transport which is observed. This is due to the presence of localised surface acceptor states as proposed by E.I. Rogacheva et al [21].

To extract the carriers from experiments on thin films and to take the surface states into account, a three-band model is used.

In another paper, N Marcano et al [17] produced 10-100 nm bismuth films that were grown on Si (001) substrate by e-beam evaporation in 10^{-7} Torr vacuum. A 200 nm-thick SiO_2 oxide was formed before depositing the bismuth . The films grown along the trigonal axis [001] perpendicular to the substrate. On top of the bismuth film, a platinum layer was deposited as a protective coating. They could extract the electron and hole carrier densities and mobilities by fitting the temperature and the field evolution of the MR and Hall resistivity. The three-band model states that each

band has two parameters. The carrier density and the mobility of the band. Moreover, the overall conduction is the sum of the contribution of each band. This can be written as $\hat{\sigma} = \sum_{i=1} \hat{\sigma}_i$ and the total resistance is given by $\hat{\rho} = \hat{\sigma}^{-1}$. Carrier densities and mobilities are extracted by fitting the data using the model. However, the model does not take into account the anisotropy in the electron mobilities that are present in bulk bismuth. This did not significantly affect their results because the films were not mono-crystalline. They also restricted the model to the interplay of the three isotropic bands. Nevertheless, the fittings that were obtained by N. Marcano et al [17] suggest that the model is already pretty reliable. The comparison of the fittings between the two-band and three-band models is shown on Figure 20. Their results about the Hall resistivity at isotherms temperatures for different fields, and Hall resistivity as a function of the magnetic field for several thicknesses are present in the annexes as Figure 64 & 65.

4.2.2 Film Thickness

Bulk bismuth is a 3D system where the electrons and holes can move in 3 different directions. In bulk bismuth, the mean-free path can reach several millimetres [23]. However, in thin films the confinement in a near 2-dimensional system has a direct impact on transport properties. The mean free path, conductivity, mobilities, carrier concentration and coherence length depend on film thickness. Several of these properties are in fact related. As the thickness decreases, the system moves from a 3D bulk material to a 2D system. The impact on the electron mean free path is easy to conceptualise. As the film thickness shrinks the possibility for the electrons to travel a great distance without meeting any borders greatly diminishes. To be able to cross millimetres of films without meeting any borders in a 20 nm thick film, the electrons would need to move in a near perfect parallel trajectory relative to the substrate, and in the meantime, not being deviated from this direction by the grain boundaries. This is of course very unlikely, in reality, the mean free path is inversely proportional to the thickness of the film. R. A. Hoffman et al [24] reported the observation that the carrier mean free path diminished when the thickness of the film decreased. Their result is presented in Figure 22a. Note that the films in their study are in the micrometre thick scale, whereas here we focus on nano-scale. However, this illustration still shows a clear decrease of the carrier mean free path for thin films compared to the bulk material. Aitani et al [10] also shows that the phase coherent length decreases linearly as the film thickness decreases. This linearity can be seen on their fitting in Figure 22b.

Conductivity is also affected by the decrease of carrier mean free path. The diminution of carrier mean free path means more collisions, this reduce the drift velocity of the carriers while travelling through the film. This causes a drop in mobility and conductivity. Another impact of film thickness is the increased electron carrier density as the thickness diminishes. This is illustrated in Figure 23 from Chun Yang [25].

Chun Yang[25] has studied the electrical properties of bismuth for several different thicknesses. He grew at room temperature three samples of 2200, 700 and 140 Å thick bismuth films using thermal evaporation on sapphire substrate covered by a layer of CaF_2. The bismuth was deposited on top of the CaF_2 layer which is not a protective layer. Two different effects are impacting the transport, the reduced drift velocity and an increased carrier density, which respectively decreases and increases the conductance. Figure 21 clearly illustrates that the finer the film, the smaller its conductance. Thus, the reduced drift velocity has a greater influence on the electrical transport

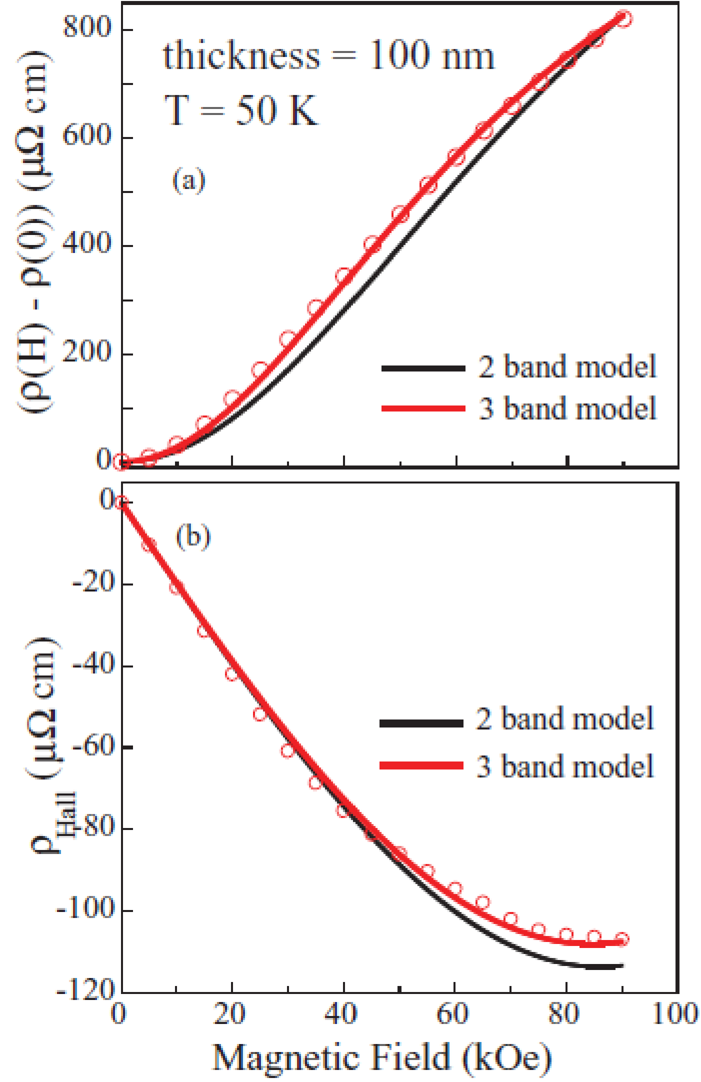

Figure 20: (Colour online) (a) Magnetoresistance (top panel) and corrected Hall resistivity ρ_{Hall} (bottom panel) versus applied field at selected temperature T = 50 K for Bi films with thickness t = 100 nm. The solid lines are determined by a fitting procedure that simultaneously includes both sets of data into a two-band (black line) and a three-band model (red line) described in the text of the original paper [17][22]. 10-100 nm a bismuth films were grown on Si (001) substrate by e-beam evaporation in 10^{-7} Torr vacuum. A 200 nm-thick SiO_2 oxide was formed before depositing the bismuth.

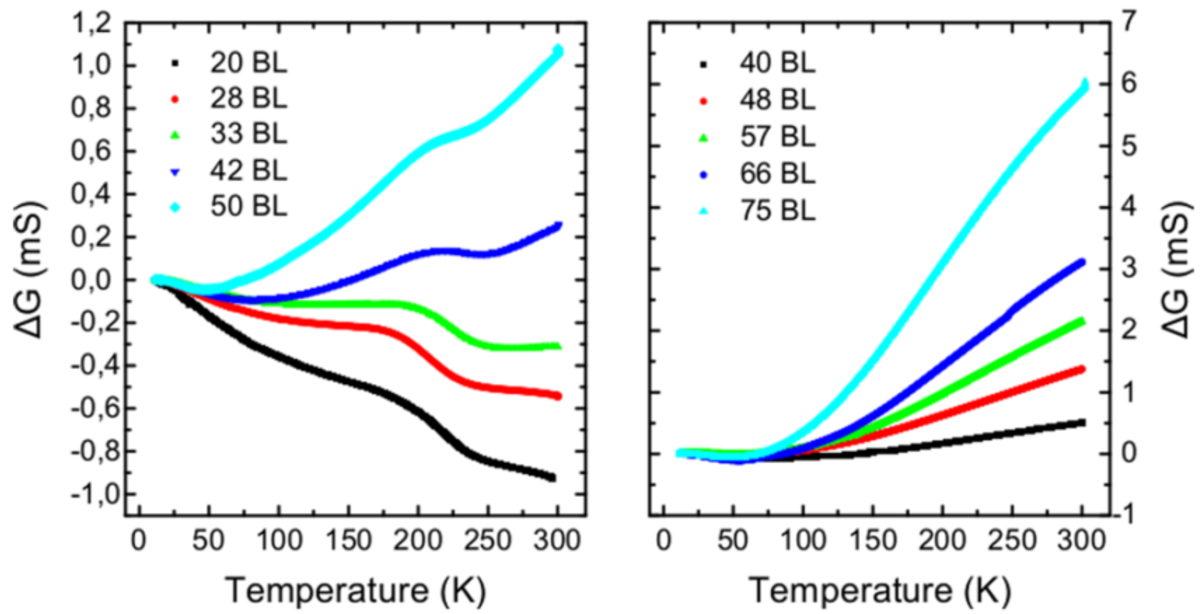

Figure 21: (a),(b) Conductance as a function of temperature for variously thick Bi(111) films. While for (b) the films were prepared on fresh Si(111) substrates, in (a) the Si(111) templates were used for multiple deposition experiments and high-temperature annealing cycles. Films are epitaxially deposed Bi on low-doped Si(111) by molecular beam epitaxy. Annealed at 450K for several minutes.

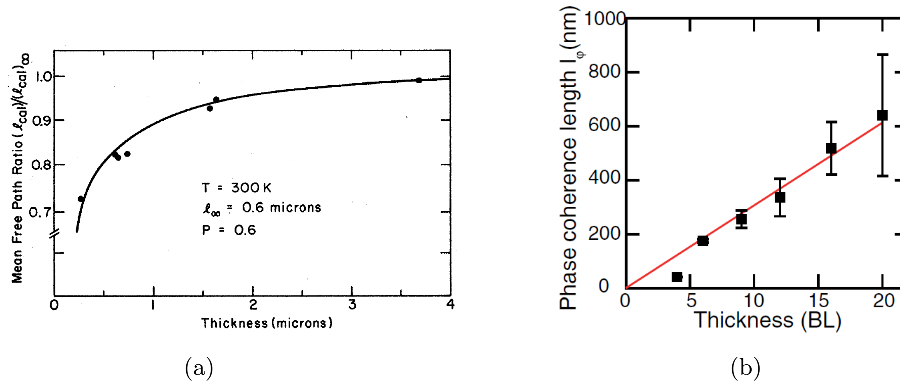

(a) (b)

Figure 22: (a) Thickness dependence of the carrier mean free path at 300 K. The curve is the prediction of the Fuchs-Sondheimer theory for l=0.6 ν p and P=0.6 [24]. (b) Thickness dependence of l_ϕ. The solid line shows the fitted curve to a linear function [10]. Samples were created in situ in ultrahigh vacuum on (111) single crystalline bismuth films of thickness ranging from 6 to 20 bilayer. These films were deposited at room temperature on Si(111) substrate before being annealed and characterized at 380K. The resulting samples were single crystalline epitaxial Bi (111) films thicker than 6 bilayer.

than the increased carrier density.

Last but not least, thin films present a limit. When bismuth is deposited on a substrate by an evaporation technique, it starts by generating nuclei that will grow and reach the coalescence stage as the deposition continues. If the deposition is stopped before the coalescence stage, (typically for bismuth films of a thickness inferior to 6 nm on silicon substrates), the film does not provide a contact between the anode and cathode, and thus the resistivity greatly increases. This electric coalescence can be seen on Figure 5a where no sheet resistance where obtained for thickness lower than 6 nm.

In short: decreasing the film thickness **decreases** the following properties:

- the mean free path of the carriers
- the conductivity
- the mobilities
- the coherent length

But increases the carrier density.

4.2.3 Temperature

Temperature is an important parameter for semi-conductors and semi-metals. Note that in this section, we talk about the temperature in which the electric measurements is carried and not the

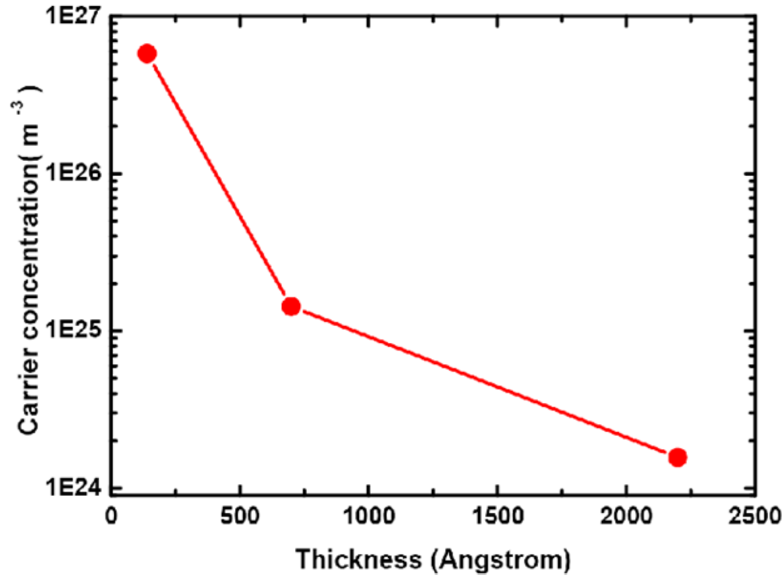

Figure 23: Electron carrier density as a function of thickness of Bi films at 4.2 K[25]. Film deposited on a Sapphire substrate that was coated with CaF_2 at room temperature.

deposition temperature at which the bismuth film was made.

Temperature influences several properties such as carrier concentration and type, the mobilities, the mean free path and thus resistivity. In metals and semi-metal, the resistivity decreases when metal is cooled down, from room temperature to a lower temperature. This can be observed on Figure 24b, in addition to this, the mobility also increases as the temperature diminishes (Figure 24a).

At very low temperatures, several important changes can be noticed. First, Hoffman et al [4] reported that for thin bismuth films, at low temperature, the majority of the carriers are holes . The temperature can modify the transport from bulk transport into transport dominated by surface states as the temperature decreases [10]. An illustration of this modification of conductance is shown on Figure 26 where Lükermann et al [18] met a transition from a bulk conductance to a surface state conductance. Their sample, a 15 BLs bismuth film deposited at room temperature on a low doped Si(111) substrate which was later annealed at 400K for several minutes. They also concluded that the observed transition at 60K means that the film turns into a semimetallic state.

Aitani et al prepared, high quality samples that enabled them to make observations of transitions in bismuth transport behaviour [10]. The samples were created in situ in ultrahigh vacuum on p-doped (1-10Ω) Si(111). Single crystalline bismuth films of thicknesses ranging from 6 to 16 bilayer (23.4-62.4 Å) were deposited at room temperature before being annealed at 380K. The resulting samples were single crystalline epitaxial Bi (111) films thicker than 6 bilayer.

In situ means that bismuth was deposited and electrical measurements were made without exposing the sample to air. In situ characterization prevent oxidation of the film. On the other hand,

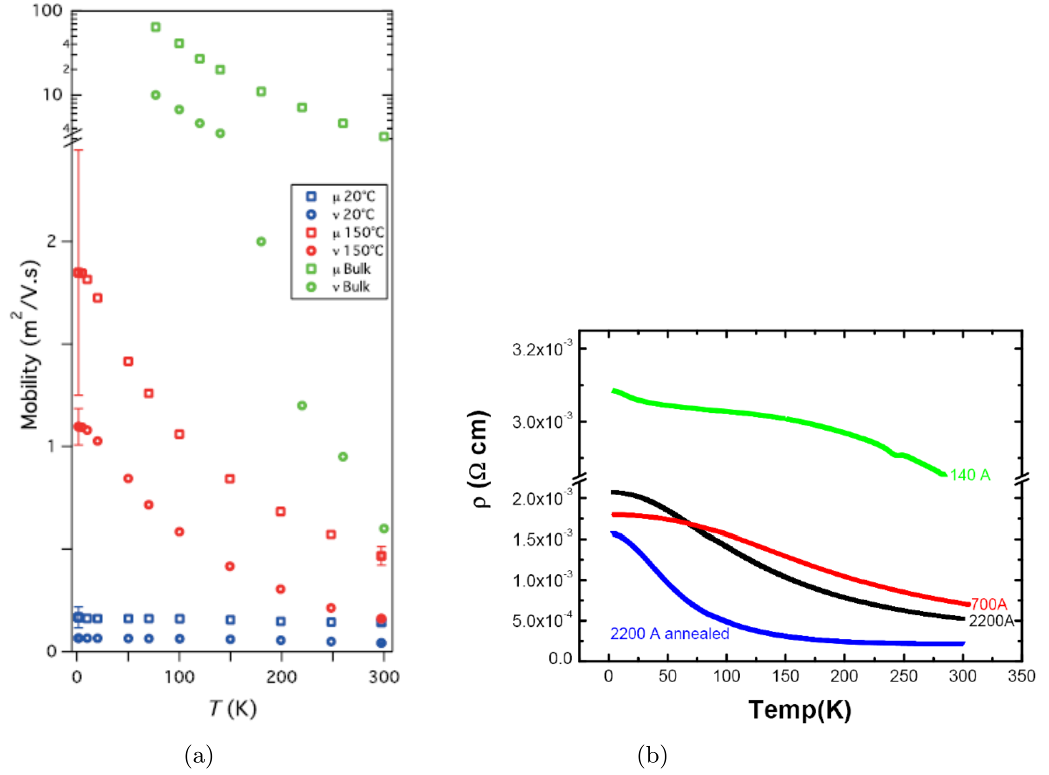

(a)

(b)

Figure 24: (a) Mobility of electrons (squares) and holes (circles) for 100nm films deposited at 20 (blue) and 150 °C(red), as a function of temperature on KCl substrate. Values for bulk Bi are plotted for comparison (green) [5]. (b) Combined resistivity vs. temperature for bismuth samples deposited on Sapphire substrates which was covered by a CaF_2 layer. The samples are respectively: 140, 700 and 2200 Å thick. bismuth 3 (140 Å) shows the highest overall resistivity, while bismuth 1 (2200 Å) initially shows a higher resistivity than bismuth 2 (700 Å) at lower temperatures. The annealed 2200 Å sample has the lowest overall resistivity [25].

ex situ measurement means that the sample was made in situ but the sample was measured outside of the deposition chamber. This exposition to air causes oxidation of the film and can modify its transport properties.

On these samples, they observed a transition from a metallic behaviour to an insulating one around 4K due to electron-phonon interaction. This transition was independent from thickness of these films as the same results were obtained for samples for 6 to 16 bilayer. Figure 28a and 28b show the variation of conductivity as a function of the temperature for Aitani samples. It has to be noticed that this dependence is quite weak for all temperatures. However, Figure 28a shows that films above 6 bilayer exhibit a metallic behaviour from 4 to 8 K (as conductivity decreases when increasing temperature). Whereas for temperature lower than 4K, they become insulators as the conductivity decrease with the decreasing temperature. The 4 bilayer film remains insulating for whole the temperature range. The 20 and 30 bilayer films exhibit a much stronger metallic behaviour over 4K (the curve is much steeper). Figure 27 also illustrates a slight increase of the resistivity

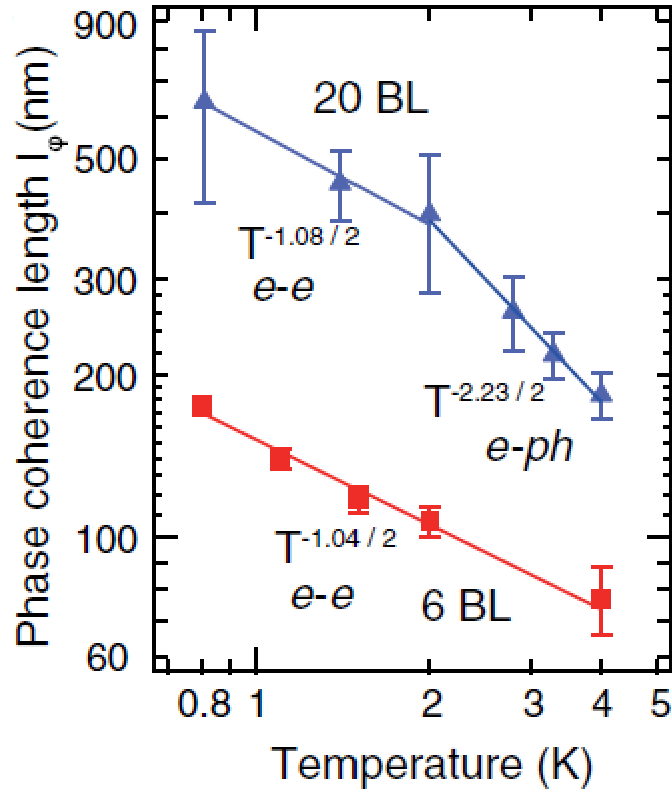

Figure 25: l_ϕ for the 6 and 20 BL films. The solid line shows the fitted curve to $l_\phi \propto T^{P/2}$ [10].Samples were created in situ in ultrahigh vacuum on (111) single crystalline bismuth films of thickness ranging from 6 to 20 bilayer. These films were deposited at room temperature on Si(111) substrate before being annealed at 380K. The resulting samples were single crystalline epitaxial Bi (111) films thicker than 6 bilayer.

as the temperature drops below 4K. The film thickness is 150 Å deposited on a mica substrate. The substrate was kept above 370K during deposition [26]. Finally, the temperature had also an impact on the phase coherence length. The coherence length decreases as the temperature increases as Figure 25 illustrates it.

In short: decreasing film temperature **increases** the following properties:

- The mean free path of the carriers
- The conductivity[2].
- The phase coherence length
- The mobility

[2]as long as Weak Anti-Localisation (WAL) does not play a significant role in the electrical transport.

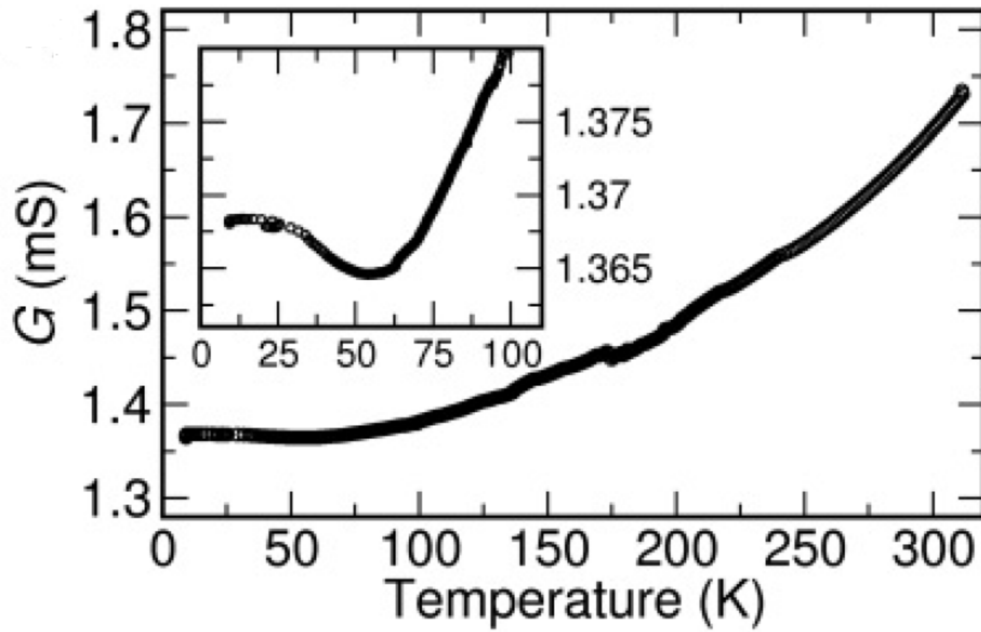

Figure 26: Conductance of a 15 BL Bi film as a function of temperature. At T = 60 K, activated transport sets in. At low temperatures, the conductance through the surface states is dominating. The inset shows a magnification of the low-temperature regime[18]. The sample is a 15-BL bismuth film deposited at room temperature on a low doped Si(111) substrate. The film was later annealed at 400K for several minutes.

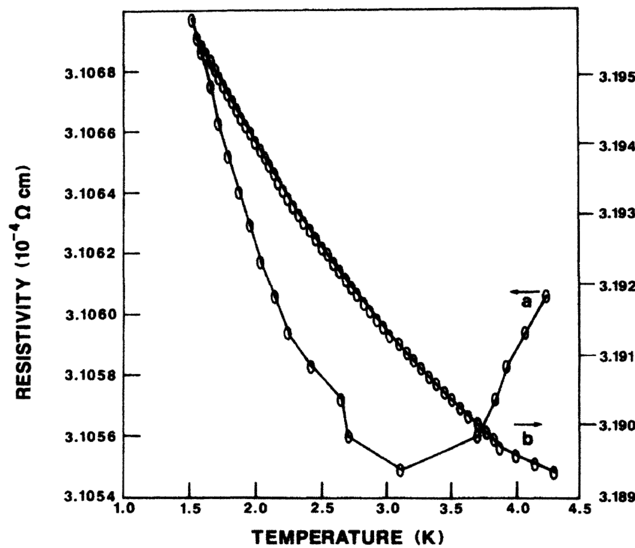

Figure 27: Electrical resistivity vs temperature. Film thickness is 150 Å deposited on a mica substrate. The substrate was kept above 370K during deposition. Curve a, zero magnetic field; and curve b, 150 Å, 20 kG [26].

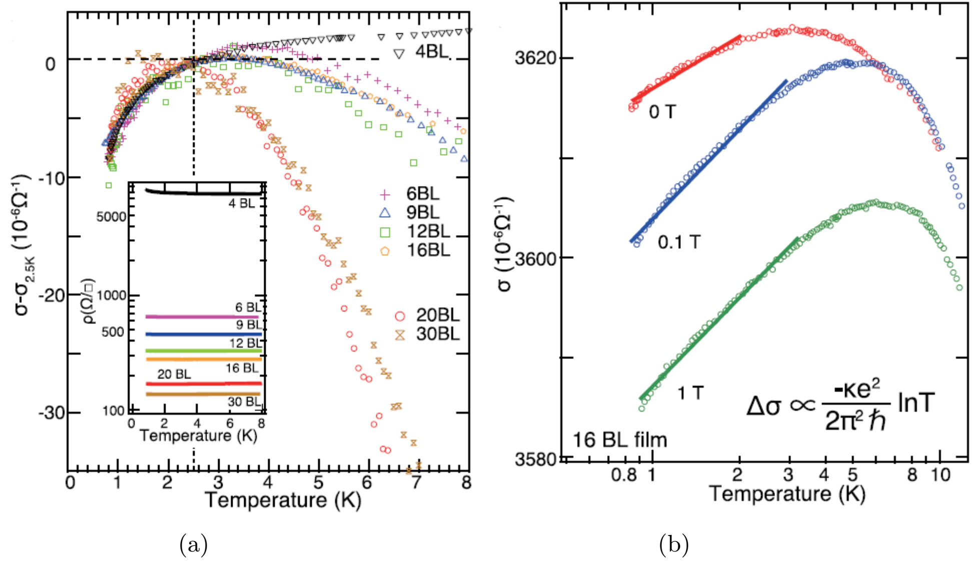

(a)

(b)

Figure 28: (a)(colour online). Temperature dependence of the change in sheet conductivity with respect to the value at 2.5 K for Bi(111) film with various thicknesses deposited at room temperature before being annealed at 380K. No magnetic field is applied. The inset shows the raw data of the resistivity as a function of the temperature. B) Temperature dependence of the sheet conductivity of the 16 BL film when applying a magnetic field. The solid lines show the fitted curves of $\Delta\sigma \propto lnT$ for the data below 2 K. [10].

Decreasing under a certain temperature, reduce the activated contribution which was named bulk transport to only keep the metallic conduction which was often called surface states transport. In addition to this, if the temperature decreases below a temperature around 4K, the resistivity starts to increase again due to weak localisation.

4.2.4 Size of the grains

Grain size can be influenced by two different factors. If the deposition rate is fast, a lot of different nucleation points are created, and the grains do not have to grow a lot before meeting other grains. Thus, a high deposition rate result in small grains. On the other hand, a substrate at a temperature higher than room temperature tends to yield bigger grains. In addition to this, it is possible to make the grain's growth even after the deposition is completed. The process is called the annealing process, by exposing the film to a temperature slightly lower than its fusion temperature. It releases constrains within the crystals and enables to form bigger grains and enhance the crystal quality [27].

A film with smaller grains has a higher resistance because the electrons are scattered on the boundaries between two grains. If grains can be bigger, less scattering occurs which cause an increase of the conductivity. This improvement of the conductivity can be seen in Figure 24b where the difference between two samples of 2200 Å thickness is obvious. Having large grains causes the roughness on the film to increase. However, the resistivity is not influenced by its roughness as the current will only be flowing through the coalesced film [28]. Kumari et al obtained grains size up to 500 nm whereas, the other grains reported before were about 50 nm [1][29]. The sample that featured that grain size was a 100 nm thick bismuth film deposited at 200 °C with a rate of 0.1 Å/s on a Si (100).

5 Setup description & Methods

This section covers the objectives of this work and its experimental setup. The results and analysis try to answer different questions that will serve as guidelines for the experimental part. A summary of these questions and respective answers will be presented in the conclusions.

on a Si (100)

5.1 Objective of the thesis

Transport properties in thin films of metal such as bismuth have been subject to numerous publications across decades and are still analyses [4, 18, 30–32].

For all the different properties of bismuth detailed in the previous section, it is still an interesting element worth investigating. This work aimed at answering several questions listed bellow:

1. The first question is to determine the conductivity of thin bismuth films and to compare eventual differences between in situ measurements and ex situ measurements.
2. The second one is to observe the behaviour of an in situ created film and to see the influence of oxidation on its electrical properties.
3. The third question is focused on the conductivity and its variation as a function of thickness and temperature.
4. The fourth question concerns film relaxation and its influence on the transport properties.
5. The fifth question is to see if quantum oscillation of conductivity could be observed as in the work of Rogacheva et al [21].
6. The sixth question is whether or not a valley of conductivity can be observed as reported by Xiao et al [19].

5.2 Components description

The evaporation setup consists of a metallizer ("Edwards Auto 306 Thermal Evaporator") equipped with a resistively-heated crucible in which bismuth pellets are evaporated and a metal deposition chamber ("FL400 Box Vacuum Chamber"). The evaporation rate of the metallizer is depending on the current going through the crucible. This current and the vacuum value are the only two parameters that could be used to control deposition. The pumping system is composed of two pumps, one primary pump and a second turbo pump. Figure 29 illustrates and details the system. The deposition and electrical measurements are carried out in situ with pressure ranging from (1.5 to 8 $\cdot 10^{-7}$ mBar). The data acquisition is done with the software Ni Labview 2017. The material for data acquisition is:

- Two "Keithley 2110 5 1/2 digit multimeter".

- One "Stanford research system model SR124 lock-in amplifier"
- One standard model K thermocouple with ranging capabilities from -200°C to 1350 °C.

Figures 30, 31, 32, 35, 33 & 34 illustrate the evaporation mask and the different components of the system. A detailed schematic of the mask with all dimensions is present in the annexes (Figure 66). The tooling factor is obtained after several depositions on the substrate and measuring the effective thickness with a Scanning Electron Microscope (SEM). An error margin of 15-20 % can be expected on the tooling factor. A SEM better suited to measure film thickness and a greater number of samples could reduced this wide error margin.

5.3 Depositions

The substrates are 24mm*24mm (100) Silicon wafers on which a 90 nm thick thermal oxide is grown. To deposit gold contacts on designated area of the sample, first a 5 nm thick titanium layer is deposited through a mask for adherence on the substrate. Then on top of this first layer, a 30 nm layer of gold is deposited through the same mask to create the contacts. Figure 36 shows a sample ready to receive the bismuth that will connect the different contacts. The bismuth is then evaporated through the mask, (Figure 30). The deposition and electrical measurements are carried in situ. This means that bismuth is deposited and electrical measurements are made at a pressure of 10^{-7} mBar without exposing the sample to air. In situ characterization prevent oxidation of the film. On the other hand, ex situ measurement means that the sample is made in similar conditions but the sample is measured outside of the deposition chamber. This exposition to air causes oxidation of the film and can modify its transport properties.

Two different deposition methods are performed:

The first set of depositions (letter A) is made on a single sample. A 10 nm thick bismuth film is first deposited at room temperature at a rate of 1.5 Å/s on the substrate. Then the temperature is decreased down to 110 K, the resistance is measured as a function of the temperature. Due to the fact that the setup, consist of metallic parts which are not insulated from the environment, the liquid nitrogen can not cool down the sample to a temperature below 100-110K. When the sample is heated back to room-temperature, a layer of 5 nm is deposited on top of the previous 10 nm. The sample is then cooled down to 110 K. Other additional 5nm layers are deposited at room temperature for a total thickness of 10, 15, 20, 25, 30 or 35 nm films[3]. For each iteration, the resistance is measured as a function of the temperature.

The second set of depositions (Letters HT, RT, LT for High, Room and Low deposition temperatures) is bismuth films deposited at a rate between [0.14-0.42] Å/s. The slowest deposition, that could be achieved with the setup is chosen to obtain a lot of data for the thickness and let the film relax while depositing[4]. The substrates and contacts are the same as for the first set of samples, but the

[3] The deposition was intended to produce films of estimated thickness: 7, 10, 13, 16, 19 and 22 nm but after looking at the effective thickness with the SEM, the tooling factor had to be modified thus changing the real thickness of the film.

[4] The relaxation is discussed in Section 2, choosing the slowest deposition speed is supposedly to let the film relax a maximum as the deposition progressed.

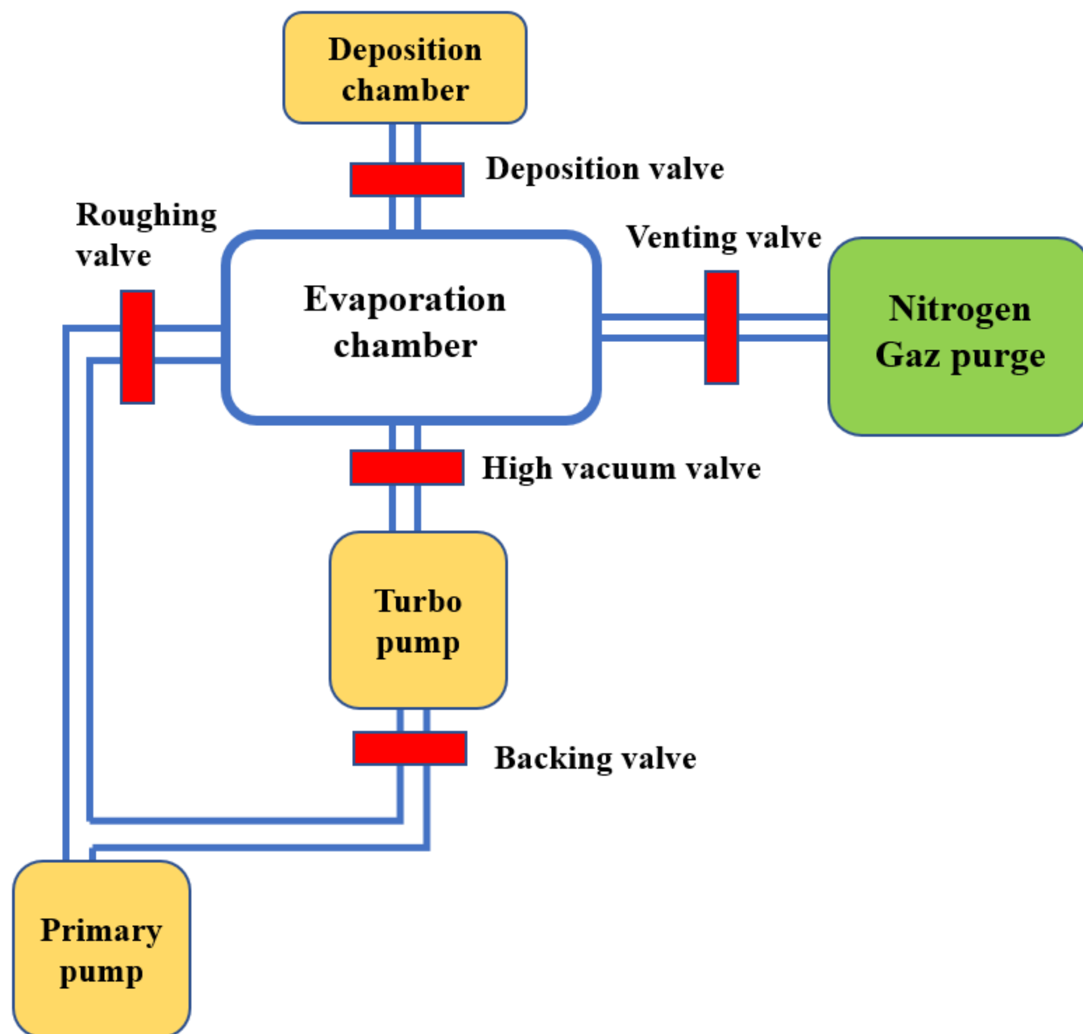

Figure 29: Pumping system: The primary pump is activated first and pumps through the roughing valve to set a 10^{-3} mbar pressure in the Evaporation Chamber. Then the roughing valve is shut and the Backing valve is open in order to set a 10^{-3} mbar pressure behind the turbo pump. When this vacuum is reached, the turbo pump is activated and the High vacuum valve is open. A 10^{-7} mbar pressure is usually reached after 3 to 5 hours of pumping. The venting valve is open when all pumps are shut and it sets the pressure in the chamber back to the atmospheric pressure. The chamber can then be open to put other pellets of bismuth in the crucible.

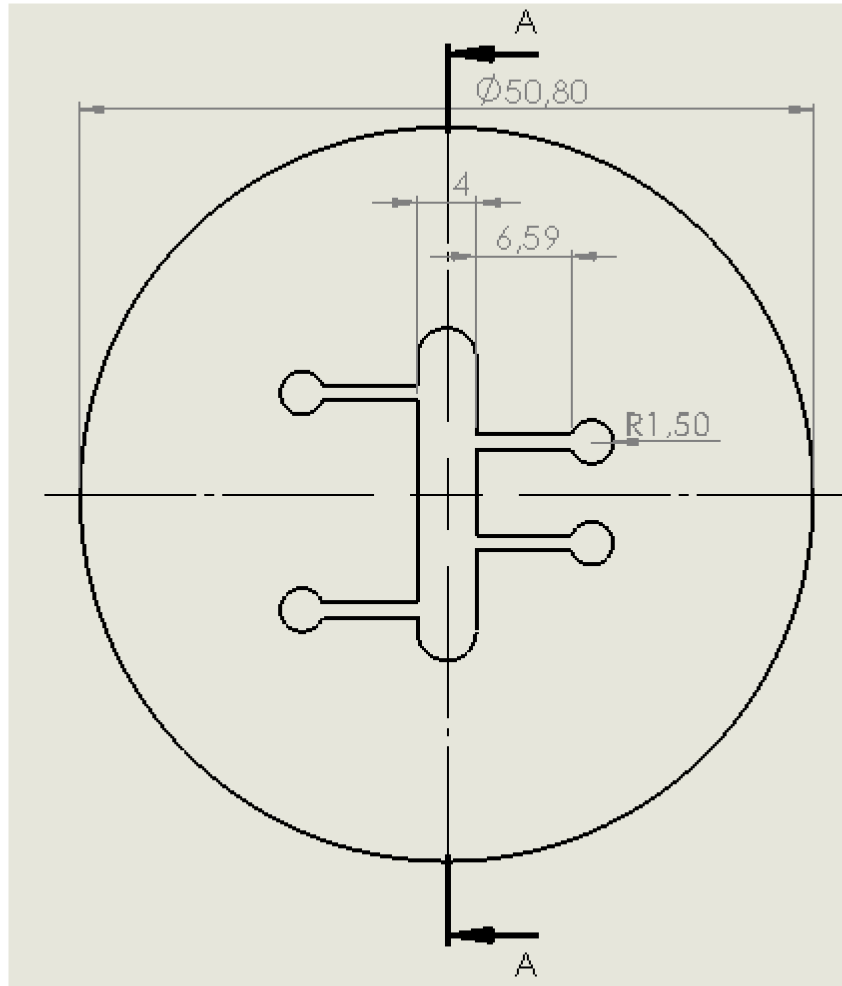

Figure 30: Evaporation mask, placed in front of the Si substrate during Bi evaporation. The units of dimension are millimetres.

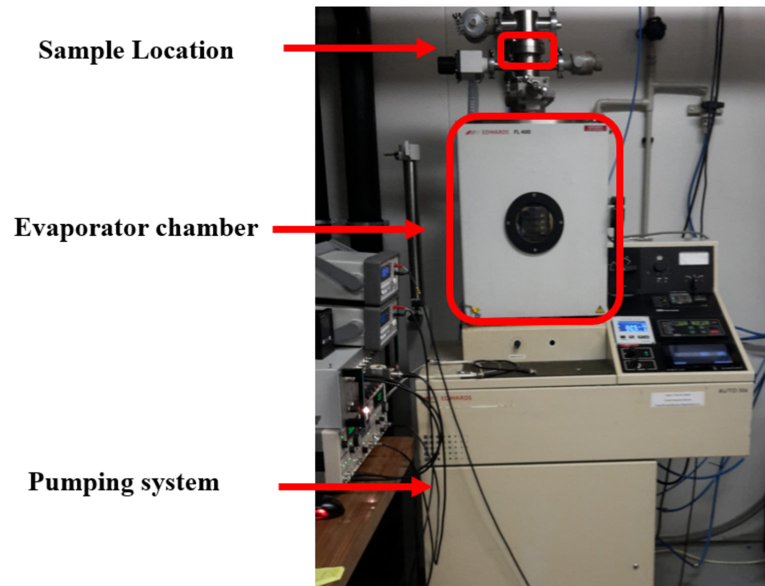

Figure 31: Evaporator used to deposit Bi thin films.

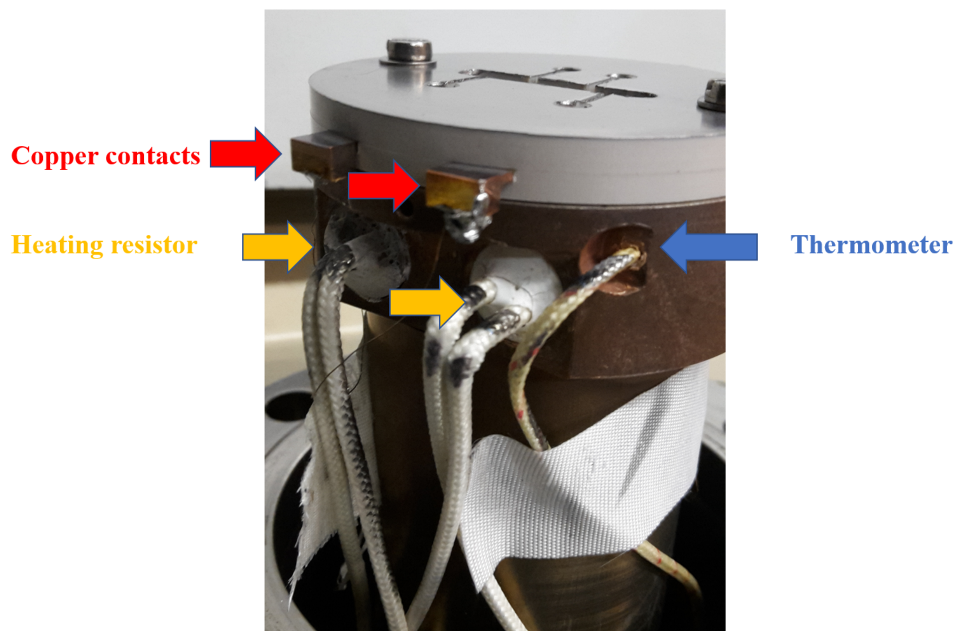

Figure 32: Support of the samples with thermometer, heating resistors and copper contacts. The copper contacts are in contact with the gold contacts that are deposited on the sample. Current and voltage measurements of Figure 41 are carried through copper contacts. The sample is heated by the two heating resistors shown on this figure.

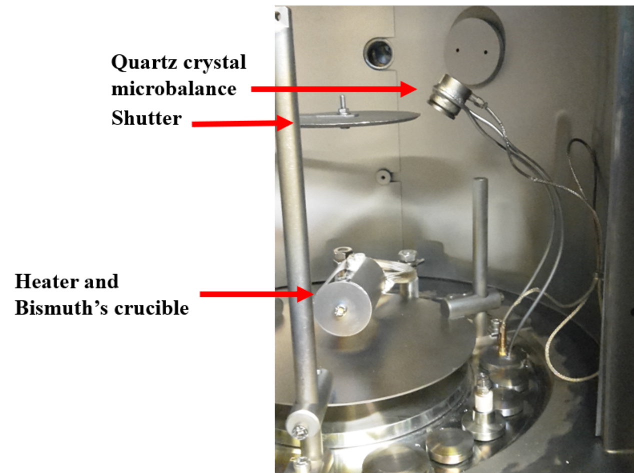

Figure 33: Evaporator's chamber with thermal source, shutter and quartz crystal microbalance. The role of shutter is to prevent bismuth from depositing on the sample while deposition rate is stabilized. Once the deposition rate is stabilized, the shutter is open and bismuth is deposited on the sample. The piezoelectric is a quartz element whose resonance frequency depends on its dimensions. As the deposition proceeds, the piezoelectric will have a variation in its frequency due to the layer of bismuth which is deposited on it. The piezoelectric can thus through computation determine the thickness of the layer which has been deposited and the rate of deposition. A tooling factor is computed by measuring the effective thickness of the film compared to the thickness recorded by the piezoelectric.

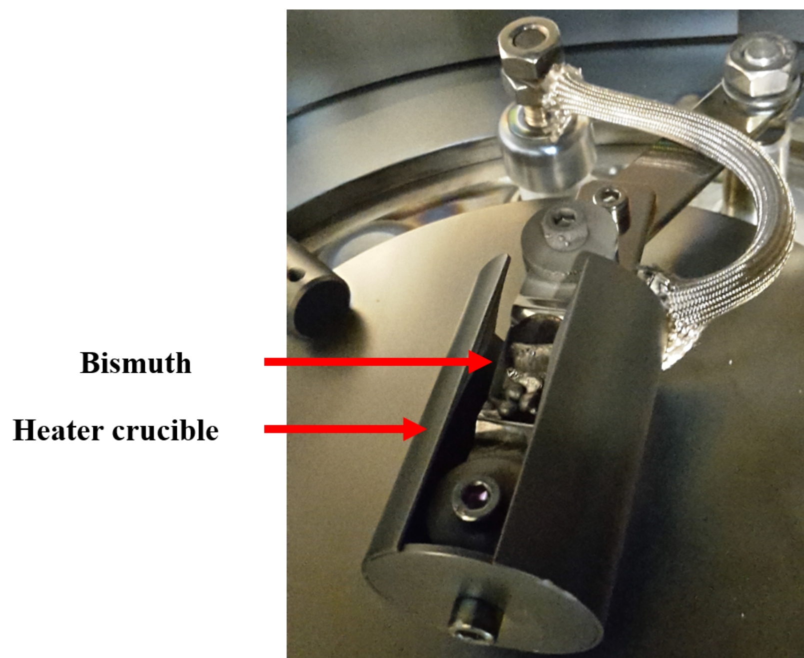

Figure 34: Heating crucible and bismuth.

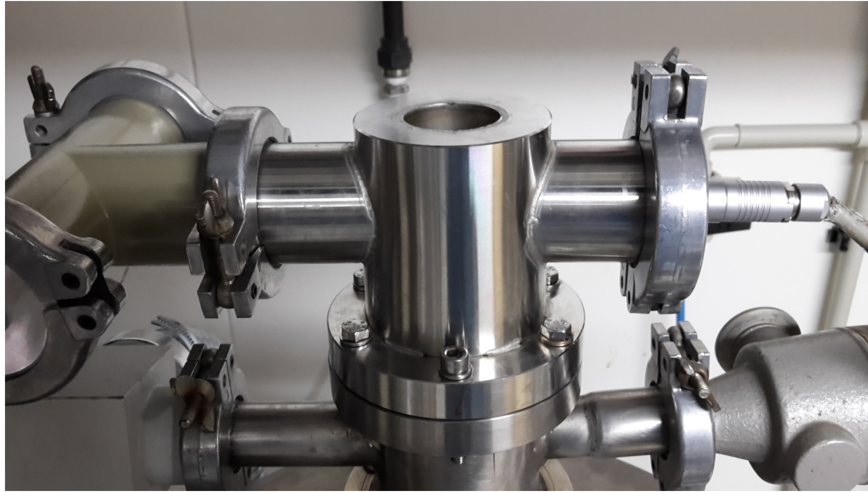

Figure 35: Cavity in which liquid nitrogen is introduced to cool the sample. This cavity is a hollow metallic cylinder which is in contact with the metallic support on which the sample is fixed. Refer to Figure 32 to see the metal part on which the sample stands.

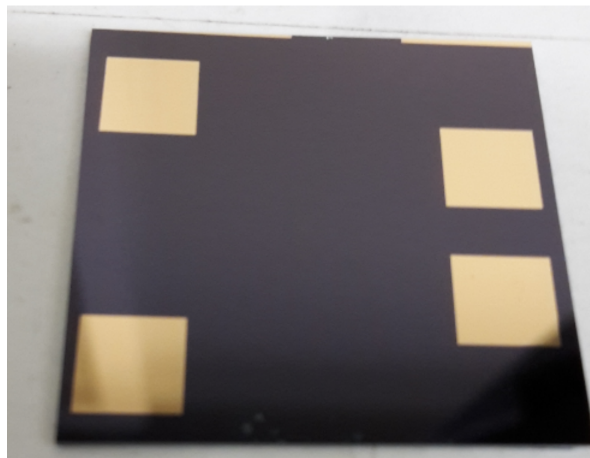

Figure 36: Sample before bismuth deposition. 24mm*24mm Si (100) with 90 nm thick SiO2 and gold contacts (30nm) deposited on top of a 5 nm Ti layer (for adherence on the substrate).

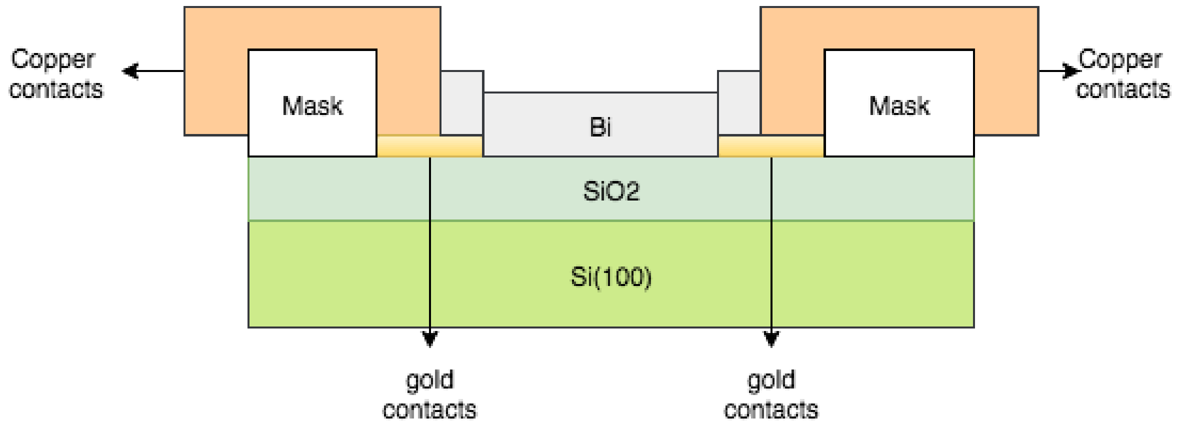

Figure 37: Cut view of the sample, copper contacts are maintained against the gold ones by screws. The bismuth is deposited and makes contact between gold layers. Once contacts are established between the 4 golds squares, the resistance of the film can be measured. An exploded view of the mask can be seen in Figure 40b.

resistance of the film is recorded during the deposition. The films LT, RT and HT are deposited respectively at 110K, 295K, 360K. Two samples are made for each temperature, other measurements are made such as recording the film's resistance evolution while the sample is maintained in situ.

A film, freshly deposited can take some time to relax its internal constraints. This relaxation has been monitored as a diminution of the resistance of the film as a function of time.

Sample O1 is produced in situ then the evaporation chamber is opened, resulting in the exposition of the sample to air. The evolution of the resistance is monitored while the sample oxidized.

The mask through which the bismuth deposition is taking place has been replaced because the first one broke during handling. The second mask (Figure 39 & 40a) is produced with the exact same pattern to deposit bismuth. The mask was entirely redesigned to be more user-friendly. The first mask required a bonding with a liquid silver glue and 100 μm gold wires. The bonding operation required to glue the gold wires to the substrate that pass each of these wires through the designated holes in the mask. This delicate operation demands a lot of time and concentration, this can be an afternoon or even a complete day. The wires could be ripped apart from the substrate when trying to pass the wires that are not yet passed through the mask.

The second mask does not require such bonding, copper contacts are directly pressed on top of the gold contacts by 2 screws. This completely bypasses the challenging bonding with the silver glue as now the mask just had to be put on top of the sample. One day of former work could be done in 15 minutes to change the sample. However the contact is not as good as it used to be with the first mask. With the first mask, 10-nm-thick films are found to exhibit measurable resistance, whereas with the second version, the films are usually around 20 to 30 nm thick before the resistance could be measured. Moreover a lot of trials are required to obtain measurements at low temperature. One hypothesis is that copper oxide is formed on top of the surface and that at low temperature it may play the role of an electrical insulator. In addition to this, the copper surface may not be as smooth

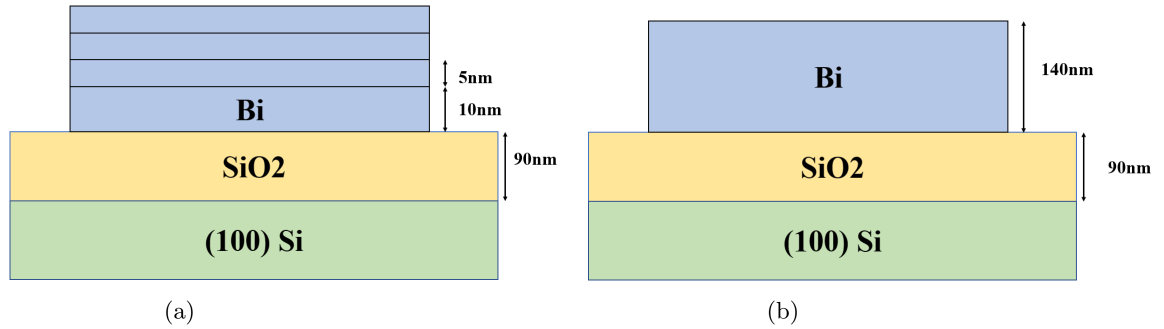

Figure 38: (a) First type of samples, a 10nm Bi layer is deposited on top of a 90nm thick SiO_2 layer on top of Si substrate. Successive depositions of 5 nm thick layers are added on top of the first layer at a deposition rate of 1.5 Å/s. Between each deposition a temperature ramp going from room temperature to 110K is performed. (b) Second type of samples, 140nm Bi films are deposited at a [0.14-0.42] Å/s rate on top of a 90nm thick SiO_2 substrate.

as before the oxidation, resulting in poor contact (copper being pressed on the substrate, but the contact with the 30 nm gold is still problematic). A solution can be to clean the copper contacts and to coat them with gold, to prevent oxidation or produce another set of copper contacts that will be larger and easier to press on the gold contacts. Another solution would be to systematically remove mechanically the oxide by abrading the copper before each bonding. Time was running short before these solutions could be implemented.

5.4 Configuration description

5.4.1 First sample series A

For all deposition configurations, the sample is contained in the metallizer and maintained in situ. The temperature probe is just beneath the sample to record its temperature (Figure 32). A current of 100 nA is injected by the lock-in at a frequency of 15 Hz between contacts 1 and 2 (see Figure 41). Until an electrical contact is obtained between the different contacts, no current can be injected. The voltage is measured between contacts 3 and 4. In this configuration, one multimeter receives the tension of the thermometer and can thus compute the temperature of the sample, while the other one receives the voltage extracted by the lock-in. The out of phase signal of the lock in is not recorded as only the in-phase signal is recorded. Looking at the out of phase signal while recording the data would have inserted out of phase values and failed to record in-phase value. The lock-in parameters were de followings:

- Sensitivity: 500 mv
- Input filter 2 dB
- Time constant 30 ms.
- Output filter 2-210 Hz

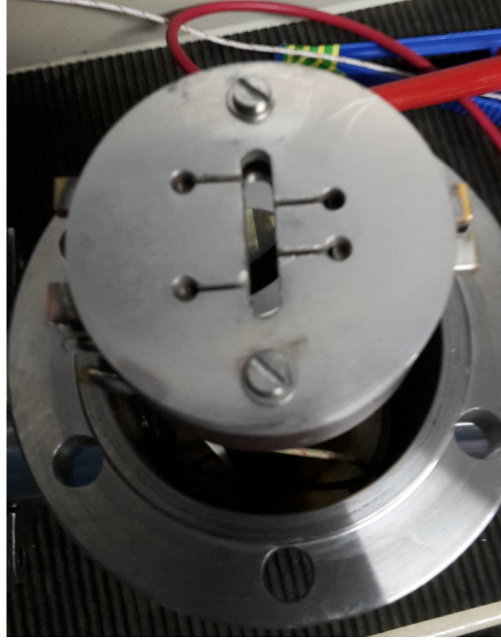

Figure 39: Mask with a sample already covered by bismuth.

5.4.2 First sample series LT, RT & HT

For the second set of depositions, 100 nA is again injected between contacts 1 and 2 and voltage measured between contacts 3 and 4. The metallizer provides an analogical output of the film thickness. This voltage measurement is illustrated in Figure 41.

5.5 Conductivity acquisition

As stated above, 100 nA current is injected in the samples. Voltage is measured between contacts 3 & 4. Sample resistance is simply extracted by dividing the measured voltage by the input current. The resistivity ρ:

$$\rho = R \cdot \frac{S}{L} \quad [\Omega \cdot m] \tag{5}$$

where S is the section of the film and L its length and R its resistance. The section of each film is the width multiplied by the thickness. For each sample, the mask has a width of 4 mm, the length is 6 mm.

$$\rho = R \cdot \frac{4}{6} \cdot thickness$$

The conductivity is then simply obtained as:

$$\sigma = \frac{1}{\rho} = \frac{6}{4 \cdot R \cdot thickness} \quad \left[\frac{1}{\Omega \cdot m}\right] \tag{6}$$

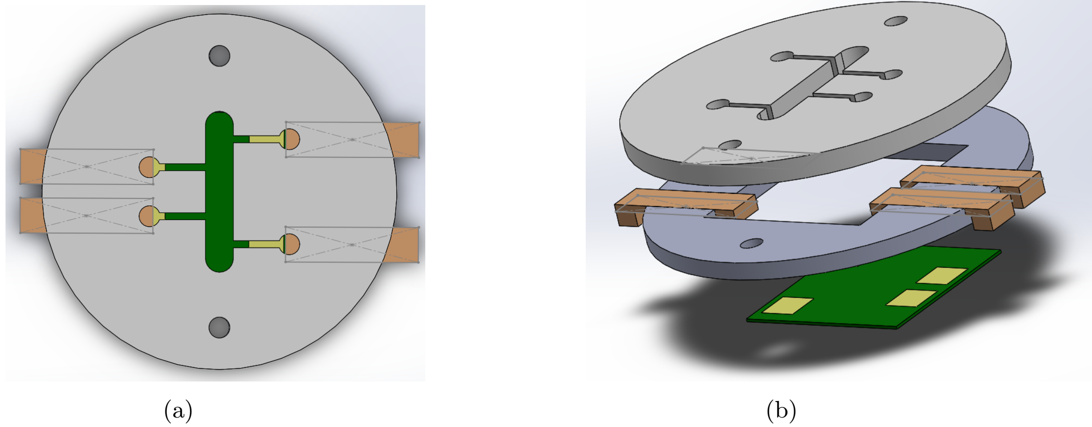

(a) (b)

Figure 40: (a) Top view of the redesigned mask (b) Exploded view of the mask and the sample. Two screws fix the mask on the metallic support and press it. This forces contact between the copper part and the gold layer.

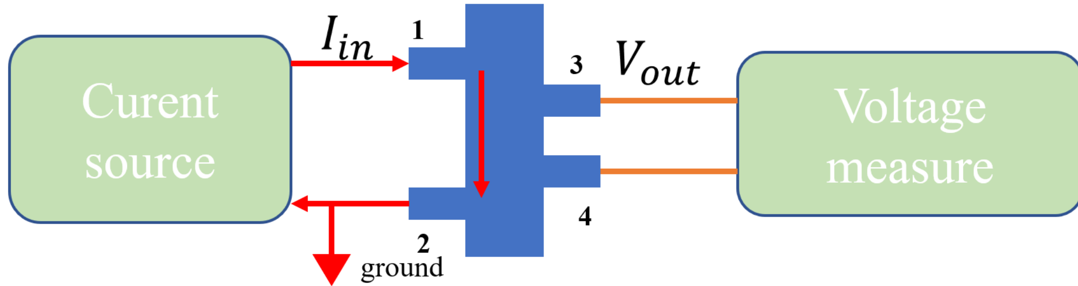

Figure 41: Voltage measurement set-up. A fixed current is injected by the lock-in. The tension is measured with a multimeter, no current passes through contacts 3 & 4.

5.6 Calculating bandgap

The bismuth exhibits an electrical conductivity (σ_{xx}) which is the sum of two contributions. The first contribution is the contribution of the surface s (σ_s) or metallic contribution and the second being the conduction in the film or thermally activated contribution[19].

$$\sigma_{xx} = \sigma_S + \alpha \cdot e^{-(\frac{\Delta E_g}{2kT})} \tag{7}$$

We define a constant b such as $\Delta E_g = \frac{2b}{d^2}$. The conductivity can thus be rewritten as:

$$\sigma_{xx} = \sigma_S + \alpha \cdot e^{-(\frac{b}{kTd^2})} \tag{8}$$

This expression contains now only two parameters which are the thickness of the film and the temperature. These two parameters will be modified in the different depositions in order to extract the band-gaps information in the films.

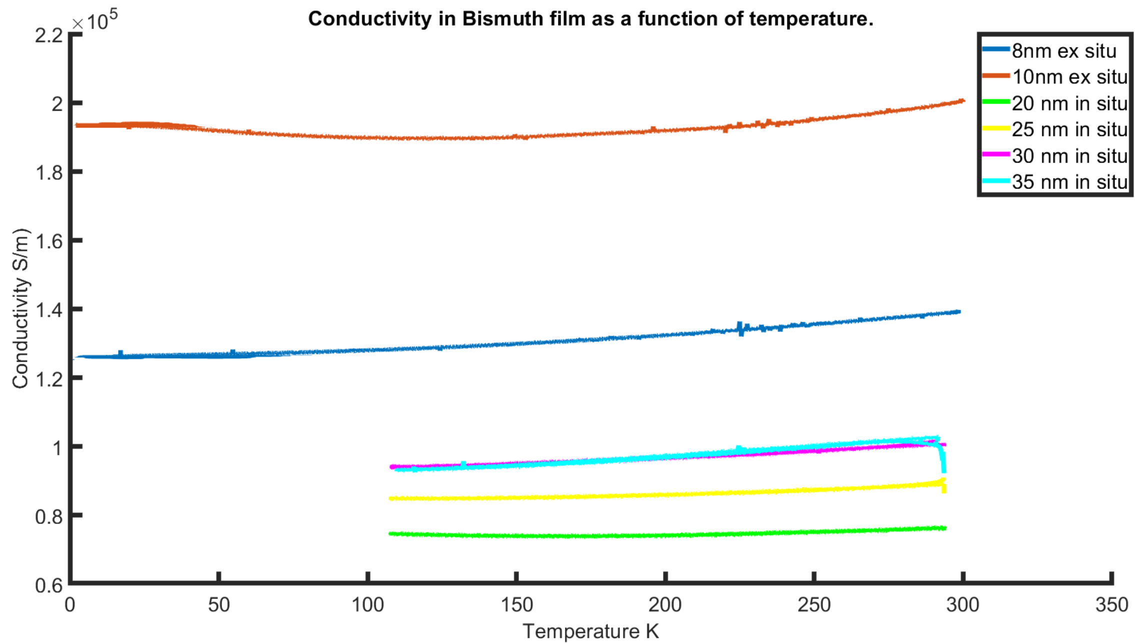

Figure 42: Comparison between in situ and ex situ results. The in situ conductivity is lower than the ex situ conductivity.

6 Results and Discussion

6.1 Question one: comparison between in situ and ex situ behaviour

For the serie A: the different results obtained are compared with ex situ measurements made by e-beam evaporation. The ex situ samples are exposed to air for about an hour before taking an electrical measurements. The layer of oxidation remains thus marginal. (Section 6.2 covers this topic). However it is important to notice that for low temperature, the value of the conductivity does not tend to 0. Therefore, it means that the samples conserved their metallic contribution from equation 8.

An unexpected result was obtained when comparing the samples in Figure 42 & 46. As the bismuth is oxidized when exposed to air, the surface conductance of the ex situ samples would be expected to be lower or about the same order of magnitude than the in situ samples. Due to experimental issues, the samples from deposition A could not be replicated. Therefore, this surprising result should be analyzed with caution. We should keep in mind that without comparison from another sample, significant conclusion cannot be drawn.

Another sample is deposited and has a thickness of 100 nm. It is compared with the two different ex situ samples on Figure 43. Here the conductivity is in the same range for the three samples. As measurement for temperature lower than 110 K was not possible to obtain on our setup, Figure 44 shows an attempt to fit the conductivity as a function of the temperature.

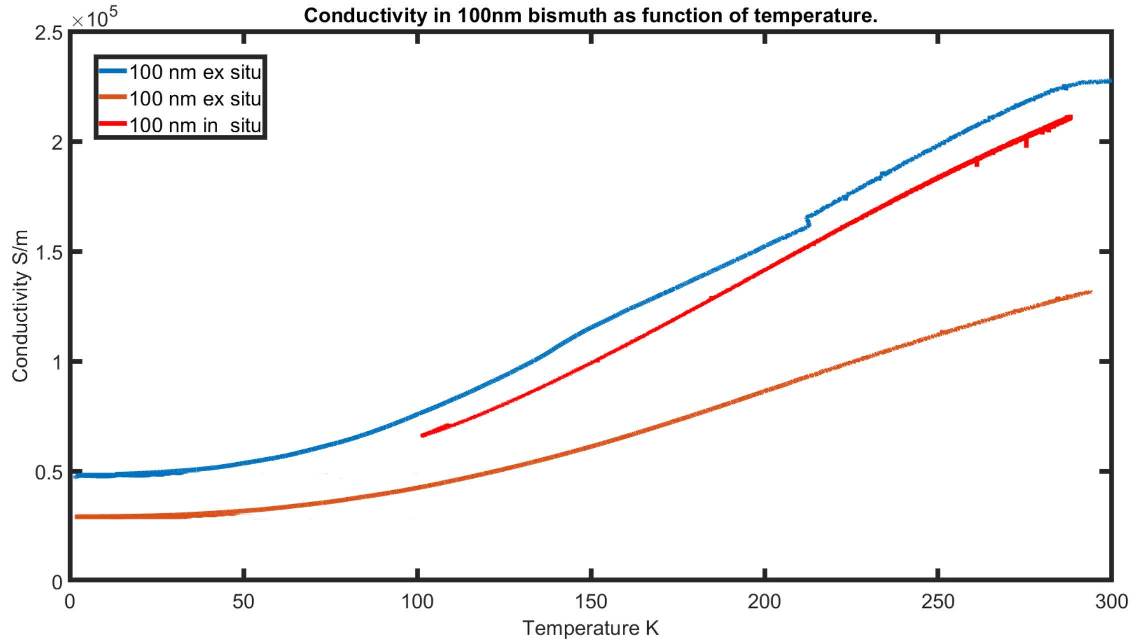

Figure 43: Comparison between in situ and ex situ results. The in situ conductivity is in the same range as the two others.

These fittings were performed based on Equation 8, surface conductivity was found to be $4.7 \cdot 10^5$ S/m for the in situ sample. The bandgaps calculated are respectively: 53meV, 68 meV and 58meV for the two ex situ 100 nm samples and the 100 nm in situ sample. These values are higher than was is expected. Section 6.3 will discuss these results and compare with results obtained in other sections.

Figure 46 synthesized these results. A clear difference in behaviour is present between the 8-35 nm thick samples and the 100 nm samples. With the conductivity of 100 nm films being lower than the conductivity obtained for 8-10 nm samples, the method used to extract conductivity detailed in section 5.5 may need to be questioned. However similar results were obtained by Xiao et al[19], Figure 45 exhibit films where the conductivity of 15-17 nm samples barely decreases with the temperature ramp whereas the 20 nm samples had a much steeper slope. Our result present films of 8-35 nm samples with similar evolution of conductivity as a function of temperature. 100 nm samples exhibit a strong dependence between conductivity and temperature, once again similar to Figure 45.

As a conclusion, Sample A has a lower conductivity than the other samples but exhibit temperature dependence similar to the 8-10nm films and literature. The 100 nm films in situ and ex situ have similar temperature dependence and conductivity value. Fitting are run to extract bandgaps for 100 nm samples. As in situ samples are thermally evaporated while ex situ samples are produced by an e-beam source, no significant conclusions can be drawn upon the influence between ex situ and in situ behaviour. Additional samples produced on the same metalliser with some measured in situ and other measured ex situ may show evidence of a significant difference. A last important point to note is that after one hour of exposing ex situ samples to air, they still exhibit important conductance at

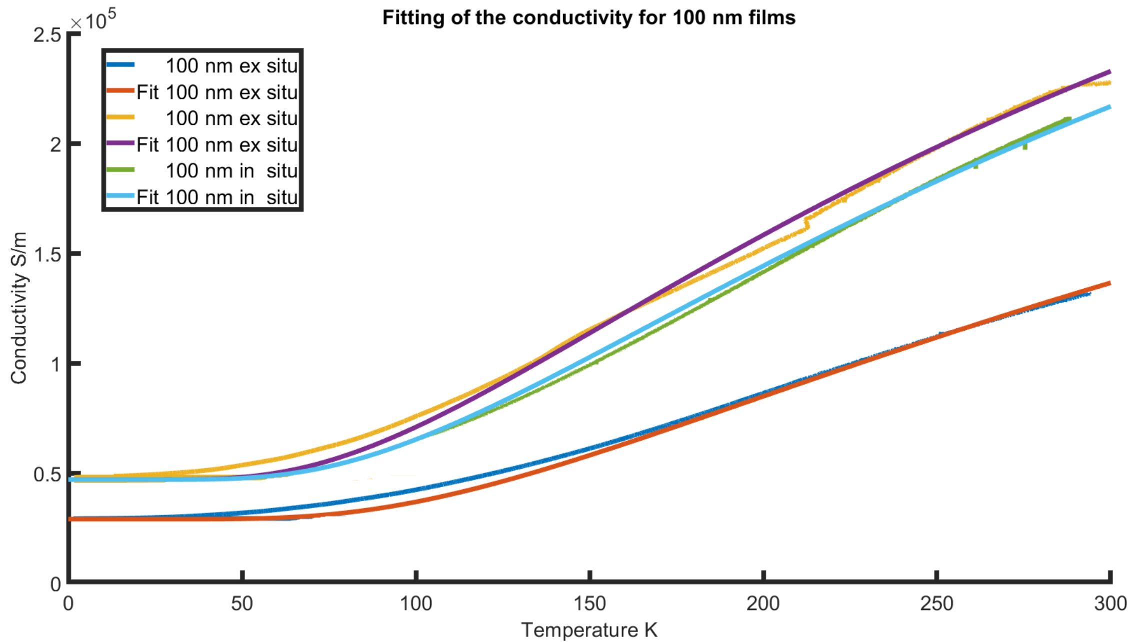

Figure 44: Fit of experimental data presented in Figure 43. The surface state conductivity of the in situ sample is estimated to be around $4.7 \cdot 10^5$ S/m

low temperature. Meaning that the surface conductance is not suppressed by oxidation.

6.2 Question two: influence of oxidation on conductivity.

A sample of 20 nm is produced in situ. When the deposition is done, the evaporation chamber is opened, exposing the sample to air. The resistivity is monitored as the bismuth is oxidized. Figure 47a & 48 illustrate the change in resistance that occurs as the sample is exposed to air. A clear increase can be seen in Figure 48. Unfortunately, the setup had a 6000 s period during which the value was not recorded. Figure 47b illustrates a value of the resistance which first dropped when exposed to air. It is difficult to conclude if this is due to experimental error of the setup combined with early relaxation. Figure 48 also exhibits similar rapid variations. Thus, without other comparisons, only resistance gradual rise is considered significant enough to answer to question 2. The resistance increases as a function of time. Figure 49a illustrates the variation of conductivity as a function of time. It can be seen that after 2 hours, the resistivity had losses 13%. But the slope afterwards is much flatter, therefore another measurement would be interesting to see what would happen on another sample without this loss of data in the early stages of oxidation.

The decrease of conductivity can be approximated by a slope with a decrease of 0.09% of the conductivity per hour. Atkinson et al [33] studied the oxidation of bismuth by ellipsometric measurements of the oxide and observed an oxidation ratez that was 0.03 nm per hour at the start and 0.01 nm per hour after four days. It tooks 9 days to reach the value of a 1.6 nm oxide. The rapid

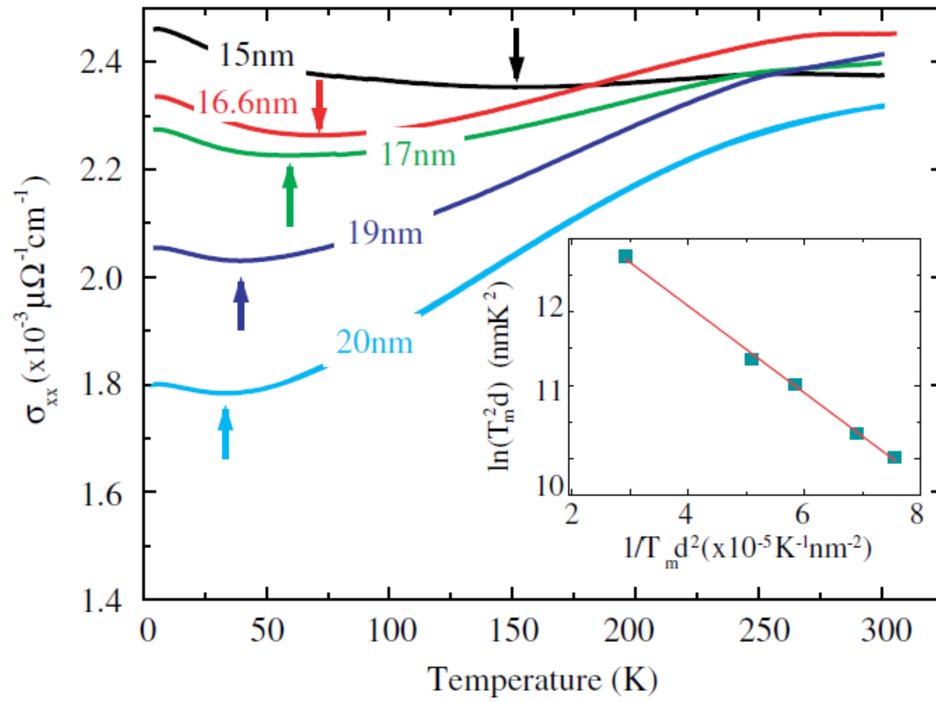

Figure 45: Temperature dependent conductivities of samples with different thicknesses. The inset shows $ln(T_m^2 d)$ as a function of $1/T_m d^2$.[19].

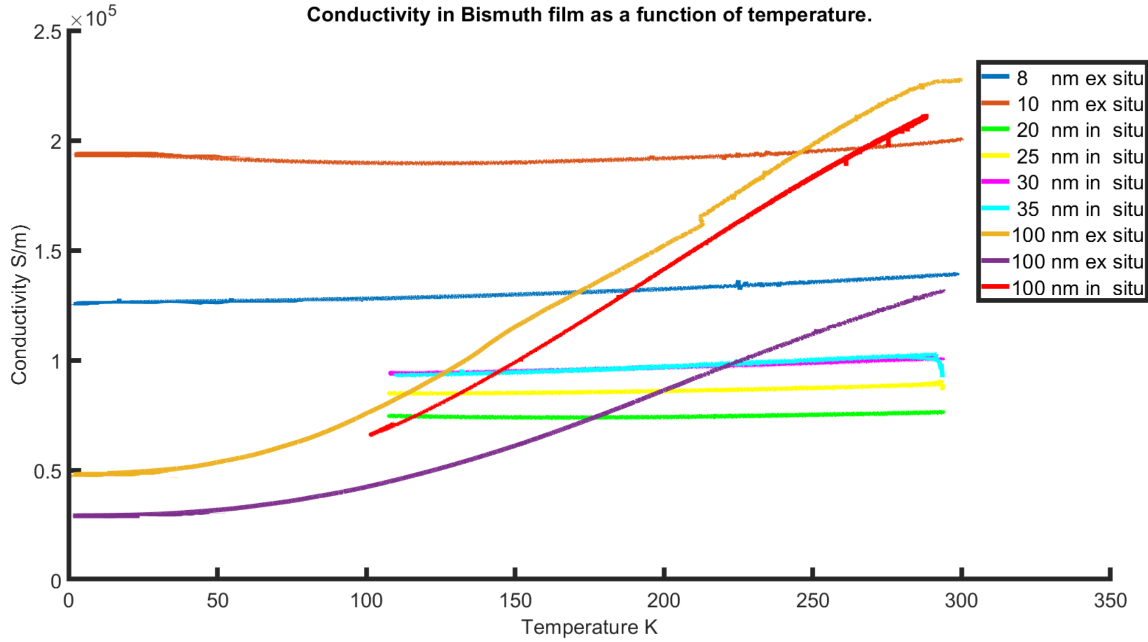

Figure 46: Comparison between in situ and ex situ results. A significant change is visible between the sample with thickness between 8-35 nm and samples having a 100 nm thickness.

loss of conductivity in Figure 49a during the moment where data were not recorded, might be due to the oxidation of the surface which eliminated surface conductivity. This suppression could be the cause of a decrease by 13 % of conductivity. However, in question one, the samples still exhibited a surface conductivity after being exposed to air for one hour. Therefore, if we still advance the hypothesis that, surface conductivity was suppressed during these 6000s, if this assumption proved to be wrong. Than a setup malfunction might be the real cause of this drop. The flat slope after the interruption of data acquisition would be the conductivity once the surface contribution was suppressed. This slope is decreasing as the oxide reduce the thickness of bismuth contributing to the transport.

By assuming that the surface state contribution was suppressed after the drop of 13% in conductivity, the effective thickness of the film can be calculated. The resistance of the film is given by:

$$R = \frac{\rho \cdot L}{w \cdot t} \quad [\Omega] \tag{9}$$

L, w and t being respectively length, width and thickness of the film. If the transport is only carried by the bulk contribution after the suppression of surface states, the bulk resistivity is assumed to remain the same for the rest of the oxidation. Taking a value of resistance after the suppression of surface conductivity enable to compute the bulk conductivity of the film. The value chosen for the resistance is 1309 Ω at 6985 s.

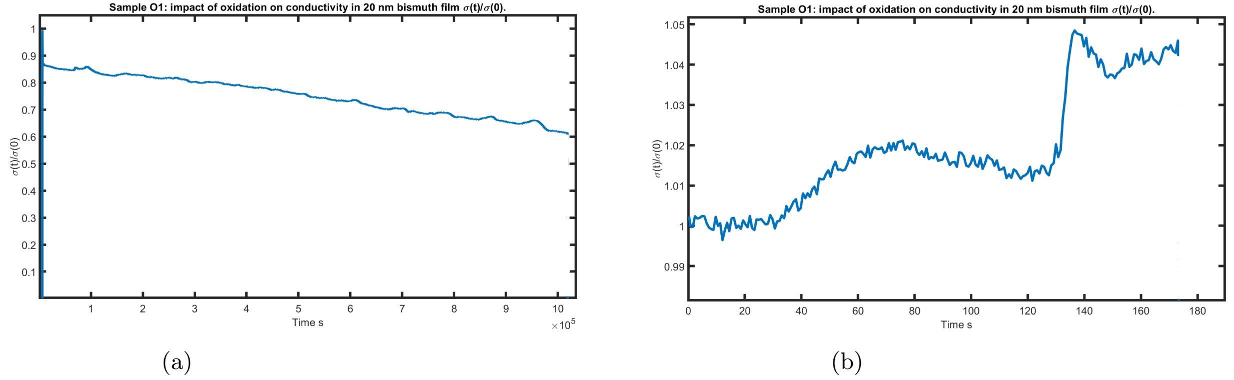

(a) (b)

Figure 47: (a) Effect of oxidation on a 20nm film on resistance as a function of time showing a clear increase. (b) Zoom of (a) just after the film was deposited. Note that graph (b) as a time span of 180 seconds on the x axis whereas the graph in a) has a time span of more than 10^6 seconds. In addition to this, a faulty contact resulted in a loss of data for 6000 s before the contact was recovered and a clear increase of the resistance as a function of time. This loss of contact can be seen in Figure 49b where no data were collected.

$$\rho = \frac{R \cdot w \cdot t}{L} = \frac{1309 \cdot 4 \cdot 10^{-3} \cdot 20 \cdot 10^{-9}}{6 \cdot 10^{-3}} = 1.74 \cdot 10^{-5} [\Omega \cdot m] \tag{10}$$

Note that we made the assumption that within 6985 s the thickness of the film remained 20 nm. The error margin of the deposition is 20 % and R. Atkinson et al found a 0.03 nm variation per hour for the oxidation of the film. Thus 20 nm is still a valid film thickness for that point.

At the end of the recording, another point is selected, its resistance is 1854 Ω at $1.017 \cdot 10^6$ s. The time elapsed between those two points is 280.6 hours. In such a long time, the effective thickness contributing to the electrical transport has been reduced due to oxidation. Computing the thickness provides the following equation:

$$t = \frac{\rho \cdot L}{w \cdot R} = \frac{1.74 \cdot 10^{-5} \cdot 6 \cdot 10^{-3}}{4 \cdot 10^{-3} \cdot 1854} = 14.1 \quad [nm] \tag{11}$$

The difference in thickness between those two points is 5.9 nm. Divided by the 280.6 hours, this gives a reduction of thickness of 0.02 nm per hour for 11 days. This is a similar result to what R. Atkinson et al [33] obtained. Figure 50 presents an attempt to fit the results of this computation for several points using linear and logarithmic functions. Results from Atkinson et al [33] are also presented. The fitting for our result is pretty poor for a logarithmic fitting.

In order to better quantify the evolution of resistance as a function of time, new samples must be prepared to compare the evolution of resistance and if a sudden drop in early exposition to air is noticed as on sample O1. This drop would confirm the suppression of surface conductivity. It is important to keep in mind that this suppression of surface conductivity is an hypothesis, the drop might be due to a setup malfunction. Moreover the model to extract the thickness of the oxide was

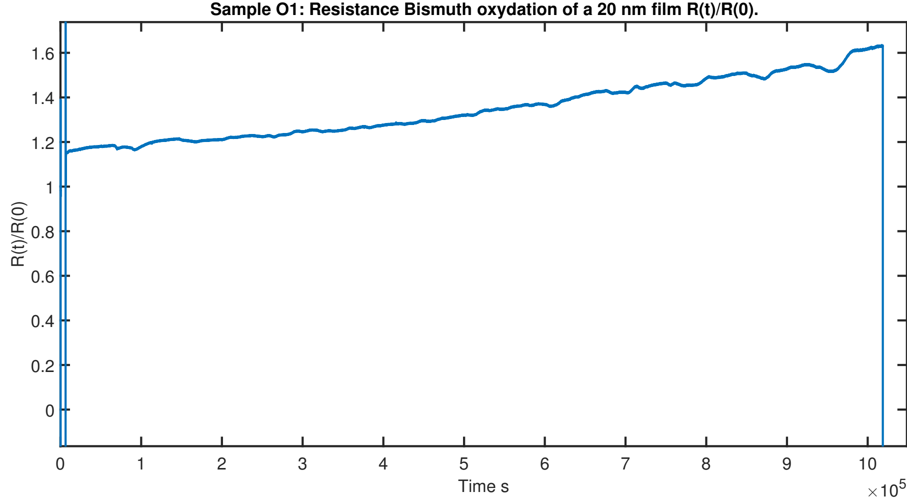

Figure 48: R(t)/R(0) evolution of resistance as a function of time of a 20 nm sample exposed to air.

based on the hypothesis that once surface conductivity is gone, the resistivity of the film remained unchanged and only the thickness of the film changed assuming that the oxide is a perfect insulator not contributing to the transport. Based on these data, one cannot affirm a strong evidence of the oxidation rate of bismuth. But with more experiments and testing the different hypotheses, a significant conclusions might be drawn.

6.3 Question three: influence of temperature and thickness of film on conductivity

The second series of samples LT, RT & HT respectively deposited at 110K, 298K & 360K for which the conductivity is recorded as a function of the thickness are presented in Figure 52. For more details on the deposition conditions, refer to Section 5.3. Hypotheses are made to extract the energy bandgap. This computation is illustrated with sample RT1 (Figure 51). In order to simplify the computations and to extract the energy bandgap, it is assumed that for thicknesses of 100 and 150 nm, the surface contribution in the conductivity can be neglected and only the bulk contribution is considered. This simplifies equation 8 in:

$$\sigma_{xx} = \alpha \cdot e^{-(\frac{b}{kTd^2})} \tag{12}$$

By taking two points at 100 nm and 150 nm with respectively $1.17 \cdot 10^5$ and $1.28 \cdot 10^5$ S/m and making the assumption that α and b are constants, the resulting system is obtained:

$$\begin{cases} 1.17 \cdot 10^5 = \alpha \exp\left(-\frac{b}{8.61710^5 \cdot 298 \cdot (100 \cdot 10^{-9})^2}\right) \\ 1.29 \cdot 10^5 = \alpha \exp(-\frac{b}{8.61710^5 \cdot 298 \cdot (150 \cdot 10^{-9})^2}) \end{cases} \tag{13}$$

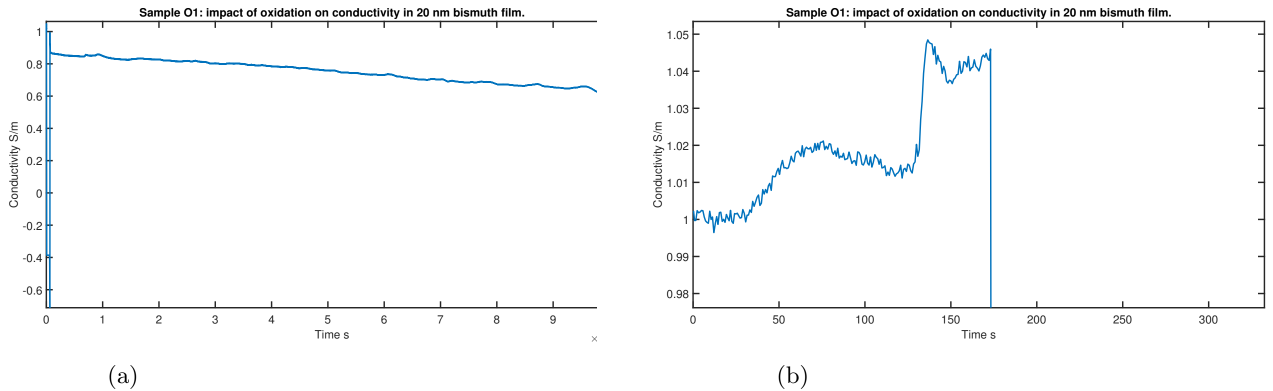

(a) (b)

Figure 49: (a) Evolution of the conductivity of the film while exposed to air. (b) Zoom of a)just after the film was deposited. Note that the graph (b) as a time span of 180 seconds on the x axis whereas the graph in (a) has a time span of more than 10^6 seconds. In addition to this, a faulty contact resulted in a loss of data for 6000 s before the contact was recovered and a clear decrease of the conductivity as a function of time. This loss of contact can be seen in a) where no data were collected.

Table 1: Bandgaps computed for 20nm and 100 nm thick films.

	Eg for 20nm	Eg for 100nm
RT1	220 meV	89 meV
RT2	70 meV	28 meV
HT1	128 meV	51 meV
HT2	145 meV	58 meV
LT2	38 meV	15 meV

By solving this system we obtain: $\begin{cases} \alpha = 1.17 \cdot 10^5 \\ b = 3.47 \cdot 10^{-17} \end{cases}$

As $\Delta E_g = \frac{2b}{d^2}$ the bandgap can then computed for the different thicknesses of the film. Table 1 resumes the value of bandgap computed for each sample at two different thicknesses, 20 and 100 nm. Note that the results were obtained under the hypothesis that the conduction was due only to bulk contribution. This assumption is not valid for 20nm films. The 100 nm value is thus more relevant. However, only values for gaps of 20 nm samples were found in the literature, this is why the bandgap for 20 nm thick samples were computed. The results from question one which provided bandgaps of 53, 68 and 58 meV for 100 nm films are consistent with the results presented in Table 1. However they all remain higher than what is mentioned literature. Here again the method to compute conductivity may not be the most appropriate resulting in these energies.

For comparison, Xiao et al [19] obtained 46 meV for a 15 nm film and 26 meV for a 20 nm film. Similarly Hoffman et al [4] obtained 40 meV for a 20 nm sample.

While samples HT and RT were about the same order of magnitude regarding their conductivity, a

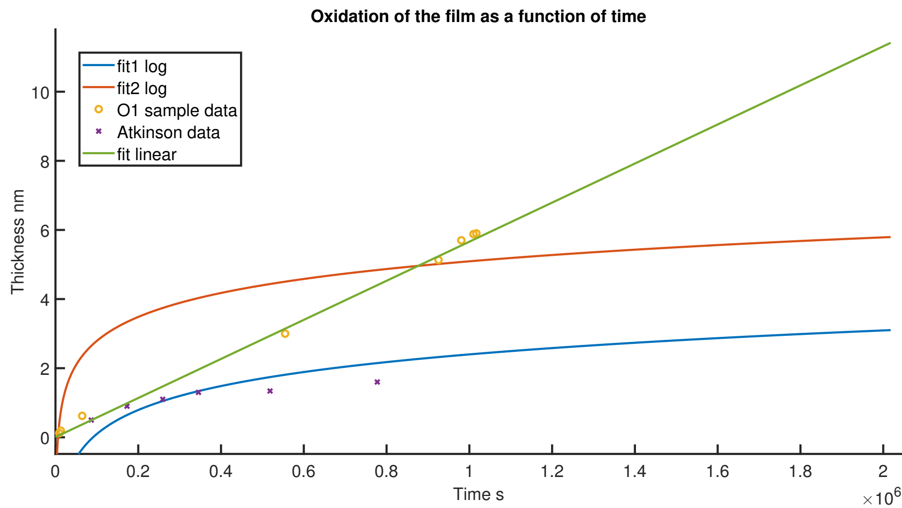

Figure 50: Attempt to fit the oxidation of the film as a function of the thickness. The results of Atkinson et al are fitted by a logarithmic function[33]. The result obtained on sample O1 tends to follow a linear fitting more than a logarithmic one. Several samples should be made to confirm this evolution of resistance as a function of the temperature. The hypothesis to extract the oxidation as a function of the resistance should be verified.

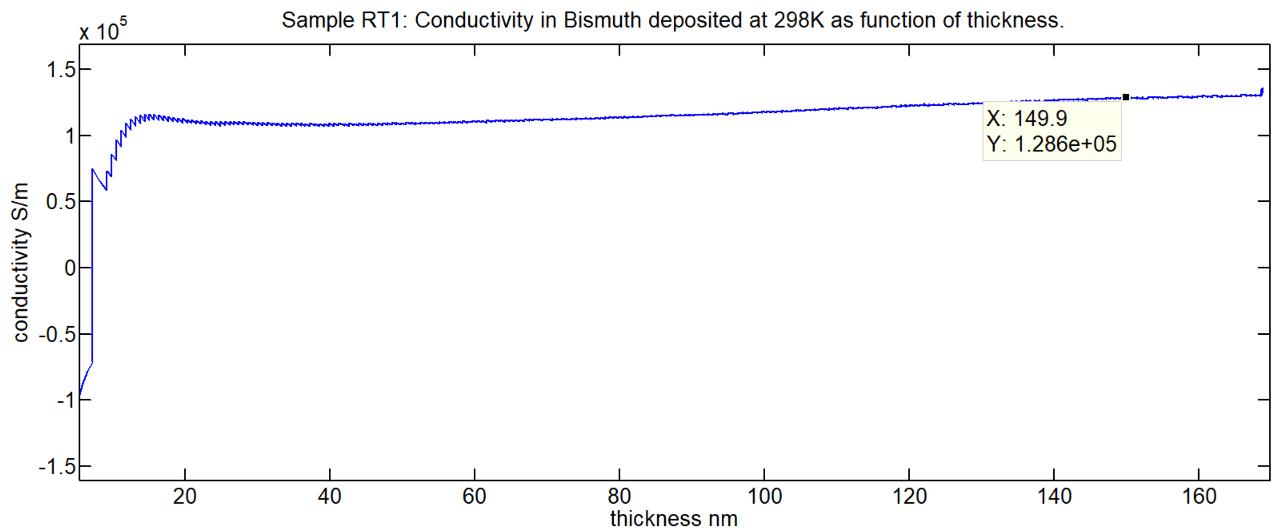

Figure 51: sample RT1 with a deposition at 298K. Conductivity recorded as a function of thickness. The 149.9 nm value is the value taken for computation.

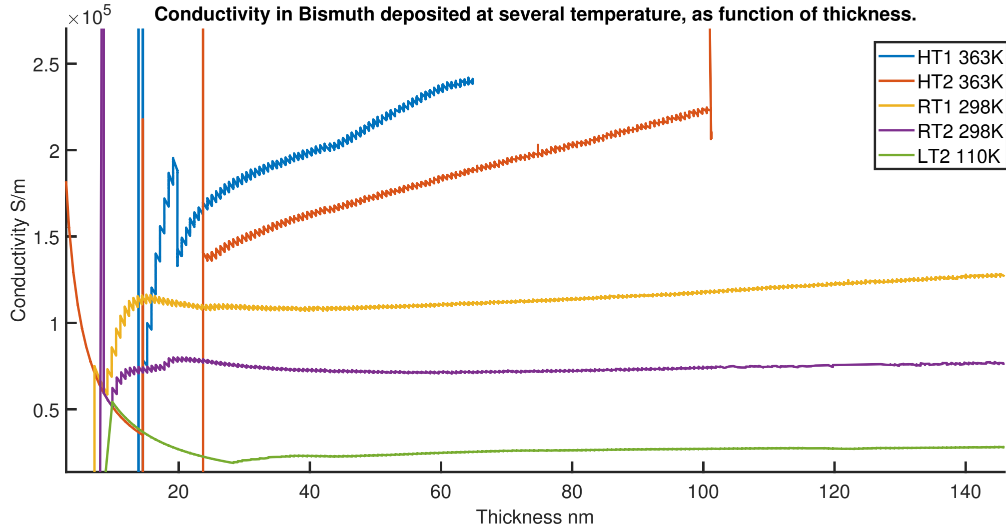

Figure 52: Comparison of conductivity between different samples deposited at different temperatures.

significant difference is noticed for the LT sample[5]. This difference can be explained by the crystalline structure which is different between the RT, HT and the LT samples. XRD pictures presented in Figure 53a & 53b. The anode source is a cobalt source, the equipment is a "Bruker 08 advanced" with a "Lynxeye" detector. To obtain this picture, the parameters were the followings: a voltage of 30kV and a current of 30 mA. A 2 θ recording was performed in the a range of 8-100. The step size was 0.02 and the time step was 2.4 s.

There is a clear difference between LT sample and the two other ones which are rhombohedral and present the same 003 and 006 peaks as in Figure 8, which presented samples thermally evaporated. The LT peak did not match any crystalline structure associated with bismuth in the equipment library. The objective of this XRD figure was less to analyse the crystalline structure of the LT sample than to rigorously show that there is indeed a difference in the crystalline structure between HT, RT and LT samples. The crystalline structure has thus a clear influence on the conductivity. In addition to this, HT samples exhibit a higher conductivity than RT samples. This can be explained by the microstructure. As both samples were deposited at low deposition rate of [0.14-0.42] Å/s the grains deposited on heated substrate could grow more. Kumari et al[1] deposited grain on Si(100) at a 0.1 Å/s at different substrate temperatures. They could show evidence of an increase of the grain size for film deposited at 100 °C over the films deposited at 30 °C.

Samples RT were deposited at room temperature and sample HT at 90 °C. Similar trends can thus be expected. Therefore, the increase of conductivity from HT samples over RT samples could be caused by this increase of grains size in the films. See Section 4.2.4 for more details on the influence of grain size on conductivity. However for deposition temperatures around 200 °C, the film structure changes again from a homogeneous film composed of laminar crystals with small voids proportion

[5] Another LT sample was produced and show similar tendency but due to lot of noise on the measure, it was not presented on this Figure. Figure 67 in the annexes presents the graphs with the sample LT1.

in the film to a bimodal particle size distribution with larger grains but much more voids[1]. This variation is expected to reduce the conductivity of the film.

As a conclusion, film deposited at lower temperature than room temperature can present a shift in crystalline structure. This shift reduce the film conductivity. Films deposited around 90-100 °C exhibit an increased conductivity due to larger grains. However for temperature approaching 200 °C, the transition in film structure causes a decrease of conductivity as a bigger void content is present in the film.

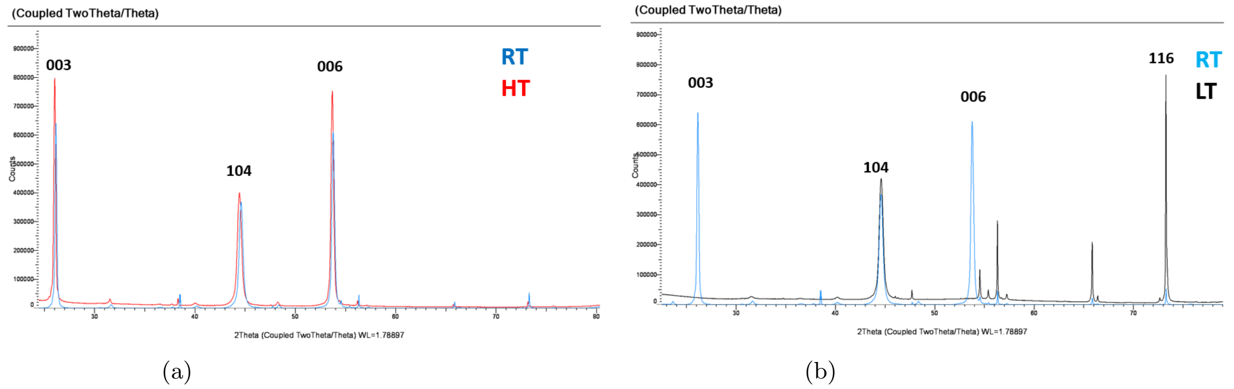

(a) (b)

Figure 53: (a) XRD image of RT and HT samples. The crystallographic orientation correspond to rhombohedral orientation. The source was a cobalt anode with a voltage of 30 kV and a current of 30 mA. (b) RT and LT samples.

6.4 Question four: influence of relaxation of internal constraints on conductivity for freshly deposited films.

A 200 nm film was deposited at room temperature. The evolution of its resistance was monitored, Figure 54 shows this evolution. When a film is deposited, internal constraints are present. As the films relaxes its constraints with time, a small variation of the microstructure results in the decrease of the film resistance of about 1% in [1-2] hours but can reach 10% if the film is monitored for 220h. The rate of relaxation is decreasing with time. For the different measurement of dependence of conductivity as a function of temperature, we did not wait for the film to relax its constraints. But the impact on these measurements is not significant as even if samples could relax for 16 h before taking measurement, the difference would lie between [2-4%] which is less than the error on the tooling factor.

Relaxation of a 65 nm film can be seen in Figure 55. One of the 4 electric contacts was suspected to have malfunctioned for this sample where a series of deposition trying to replicate serie A. Therefore the results are not presented in Section 6.1. But as the sample exhibit similar behaviour as the 200 nm one, it was decided to present it as a comparison.

The 25 nm film from set A was also let to relax after its temperature ramp. Figure 56 illustrates the relaxation of the film after the temperature ramp.

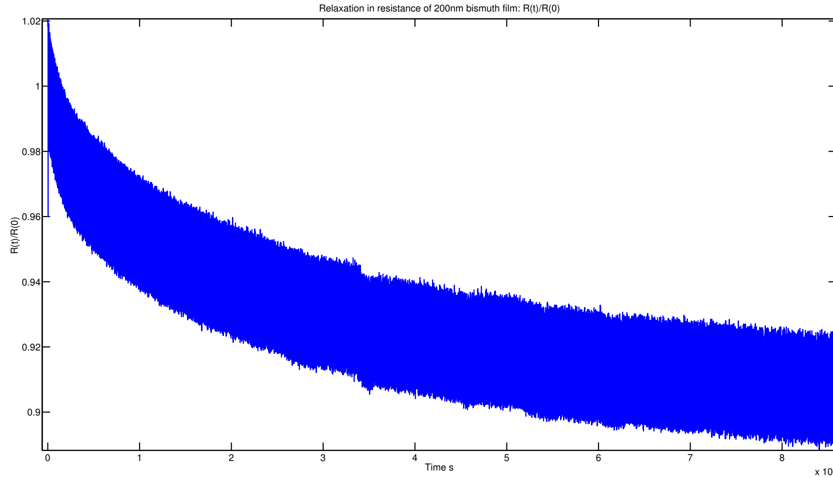

Figure 54: Resistance evolution in a 200nm film which relaxes its internal constraints.

A 50nm sample deposited at room temperature for which two temperature ramps were carried out exhibits exactly the same resistance pattern for each cycle. It was concluded that the temperature ramp had no significant impact on the film microstructure and on its conductivity before and after the ramp. Figure 57a compare the evolution of the conductivity as the films relaxes. The conductivity was fitted to obtain an upper bound approximation and to quantify the evolution of the relaxation. If the approximation is correct and relaxation continues at the same rate, it would take more than 1100h to obtain a 15% increase of conductivity. The impact of relaxation remains thus a small contribution and cannot significantly change the conductivity of the film.

6.5 Question five: observation of quantum effect in conductivity and comparison with results from literature

Figure 59a & 59b show films which exhibit oscillations in the value of their conductivity as function of thickness. For the samples deposited at room temperature) Both of them present two bumps between [10-15 nm] for the first one and [20-25 nm] for the second one. After these two bumps, conductivity remained with a constant slope. Rogacheva et al [21] thermally evaporated bismuth films at a [1-3]Å/s rate on mica substrate at temperature of 300 and 380k. Their results are presented in Figure 62. They report that their samples had a trigonal axis normal to the substrate. Their conductivity is comparable to our results. However, they report large oscillations for sample that were deposited at high temperature. This behaviour was not observed in our sample. Moreover the fitting seems to be an interpolation of the different points. This high frequency of oscillation and their amplitude make us doubtful of the fitting. By neglecting one or two outliers and changing the interpolation fitting to a different one, a large bump could be obtained with the different points. This could be much closer to the sample obtained at 300K. The bismuth structure do not exhibit drastic changes between a deposition temperature at 300 or 380K. Therefore, the sample interpretation of the different points on Figure 62a) and especially their fitting should be considered with caution. Our

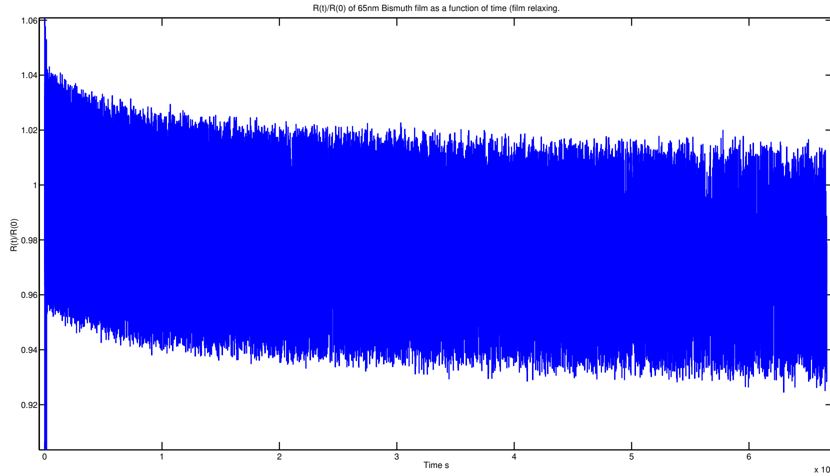

Figure 55: Resistance evolution in a 65nm film which relaxes its internal constraints.

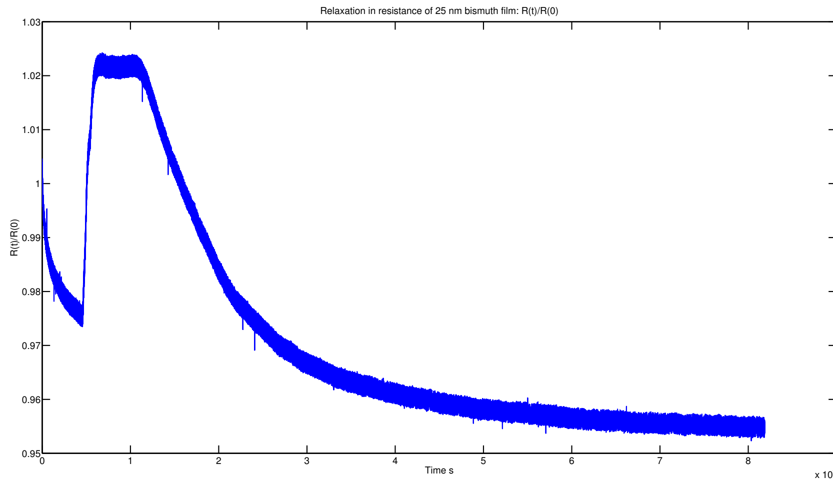

Figure 56: Resistance evolution in a 25nm film which relaxes its internal constraints. The sample was subjected to a cooling ramp which did not significantly modify the decrease of resistance due to the relaxation of constraints.

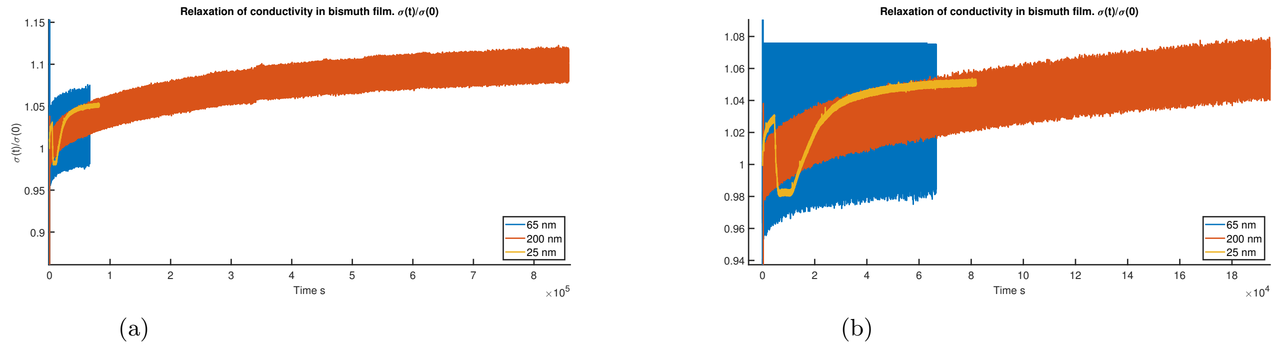

(a)

(b)

Figure 57: (a) Conductivity evolution as the film relaxation occurs.(b) The larger time span was for the 200 nm.

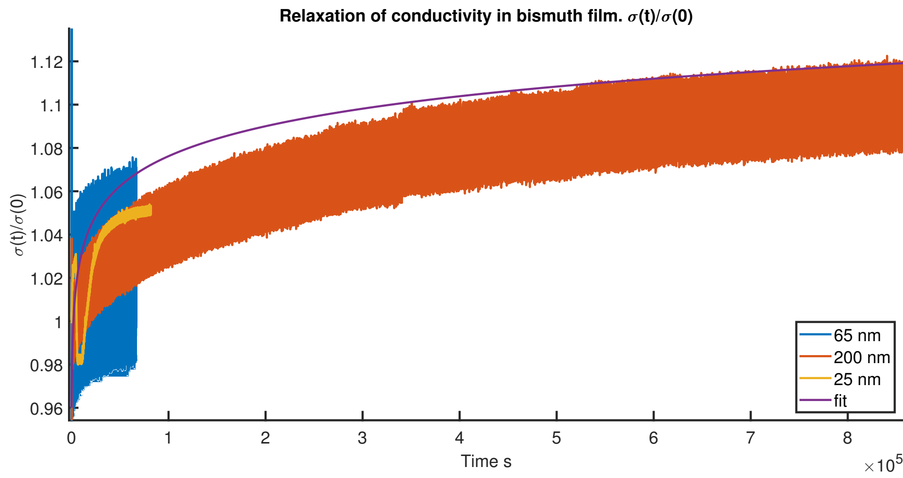

Figure 58: Conductivity with a logarithmic fit as a upper bound. The fit is supposed to match the evolution of the conductivity during relaxation.

HT samples do not exhibited large oscillations as their fitting suggested. However, some oscillations might be present on sample HT1 with two large bumps between thicknesses of [20-45 nm] and [45-65 nm], the second sample did not replicated those results. Additional samples with data recording for thinner thickness might be able to show these oscillations.

On the other hand, the fitting obtained for 300K is pretty similar to our result. This fitting is not an interpolation this time and only presents one large bump of conductivity. The noticeable difference is that in our sample, the RT bumps were obtained at [10-15nm] and [20-25 nm] whereas in their result this bump was obtained more around [40-50nm].

Oscillations in conductance are also obtained in a sample deposited a 110K. This time an oscillation can be seen around 40 nm, 70nm and maybe 120nm. As only one sample at this temperature with clear data could be recorded, it is difficult to conclude the existence of three oscillations. Other

samples may give proof of this trends.

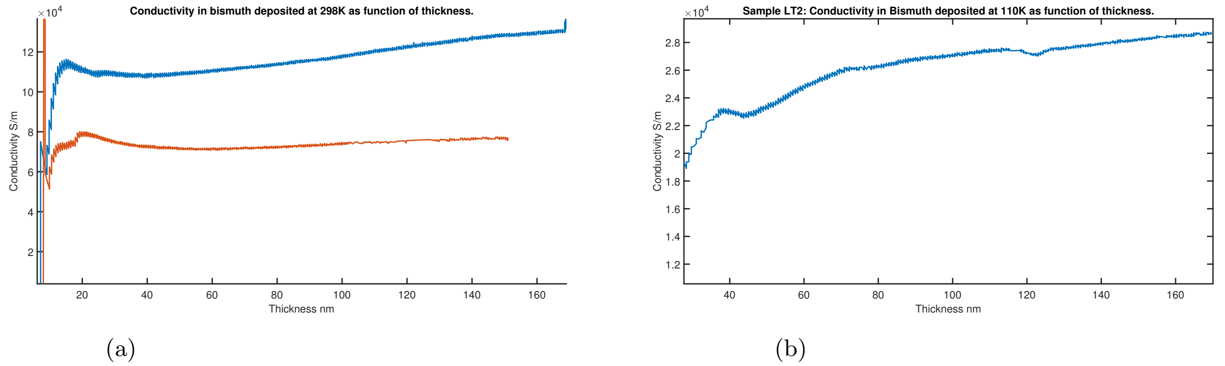

(a) (b)

Figure 59: (a) Conductivity as a function of thickness for samples deposited at RT. Oscillation in the conductivity can be observed for both samples. (b) Conductivity as a function of thickness for samples deposited at LT.

Oscillations of conductivity are quantum size effects which manifest themselves when certain conditions are met. $\lambda_F/d \geq 1$ (with λ_F being the Fermi wavelength). Furthermore, it is required that the electron mean-free path remains superior to d, the thickness of the film.

The QSEs disappears if the crystallites are smaller than the film thickness. For such crystallites, the electrons are scattered on the grain boundaries and no phenomena are observable anymore.

As a conclusion, oscillations similar to what was obtain by Rogacheva et al were obtained for samples deposited at 300K. However, samples deposited at high temperature did not exhibited large oscillations as their fitting suggested. Additional samples in larger thickness range might correspond to the oscillations that the fitting proposed for deposition temperature of 380K. Until testing of these samples, we remain doubtful on this fitting.

6.6 Question six: valley of conductivity

As explained before, the conductivity in thin bismuth film is the sum of two different contributions, one being the metallic channel, the other being thermally activated channel.

$$\sigma_{xx} = \sigma_S + \alpha \cdot e^{-(\frac{b}{kTd^2})}$$

However, according to this equation there is a temperature where the two terms are comparable in magnitude. The result is a valley of conductivity. The position of this valley is dependent on the film thickness. Figure 45 illustrates the valley of conductivities obtained by Xiao et al [19]. Similar behaviours were obtain on three samples but not on the others. These samples are presented in Figure 61a, 61b & 63.

It is surprising that only 3 samples exhibited this conductivity valley while the others never presented this inflection point. An explanation can be found to justify this fact: sample produced in

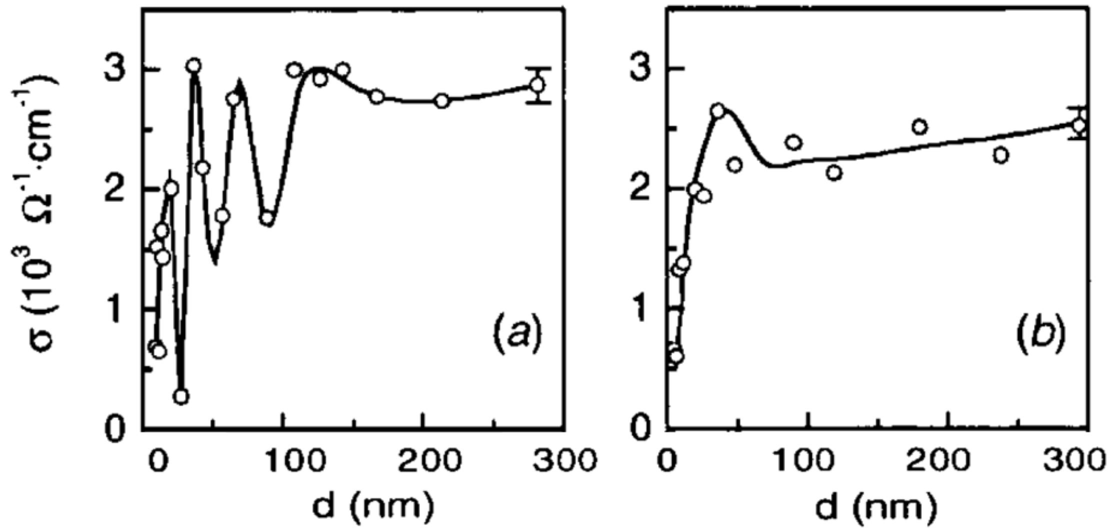

Figure 60: Conductivity as a function of the thickness. Results obtained by Rogacheva et al [21]. The samples were bismuth films deposited by thermal evaporation on mica substrate at a rate between 1 and 3 Å/s. The sample a) was deposited at 380K and sample b) at 300 K.

situ could not be cooled down below 110 K. The temperature associated to this valley of conduction may have simply been to low to be reached with the in situ samples. For ex situ samples, a problem for data treatment was not resolved in due time. This problem made several data set to be inexploitable and caused loss of precision for low temperature conductivity. This means that this valley of conductivity might be present on other samples but due to data treatment, we were not able to show clear evidence of it.

As a conclusion, valley of conductance is present in several of our samples and temperature associated with it could be given. Other samples did not exhibited it, but this could be due to temperature ramp limitation and problems in data treatment.

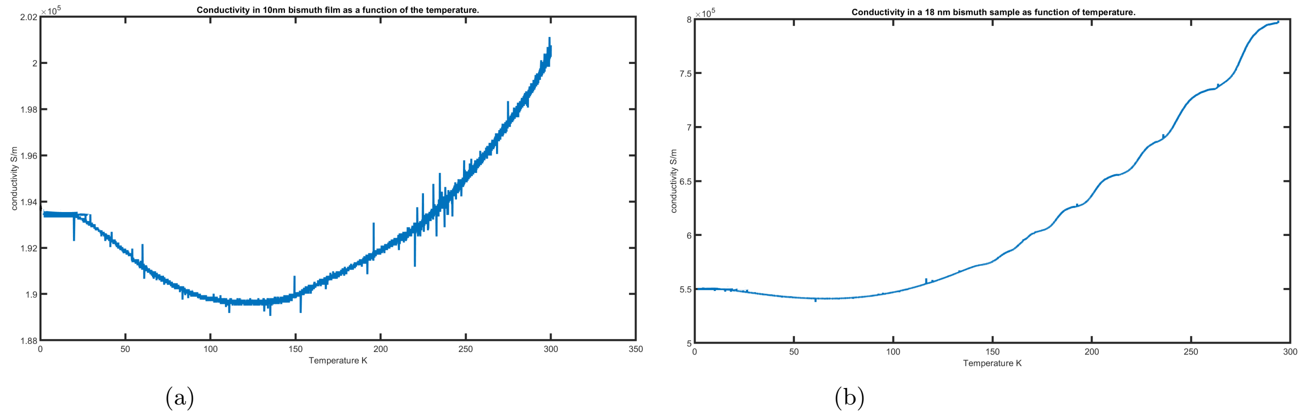

(a) (b)

Figure 61: (a) Conductivity as a function of temperature for 10nm sample with a conductivity valley. The minimum is for T=120K. (b) Conductivity as a function of temperature for 18nm sample with a conductivity valley. The minimum is for T=66K. Both measurements were made ex situ.

7 Going further

The experimental part of this thesis was carried out in six month time. Over that period, delays accumulated from different sources as making the experimental setup operational (8 weeks), receiving silver glue for the bonding process (5 weeks), designing and machining a new deposition mask (3 weeks). Due to these delays, the number of samples that could be prepared in due time was limited. Several different behaviours of thin films were investigated but without a large number of samples, no significant conclusions could be drawn.

We present here a list of different recommendations for the pursuit of the project. We also detail why these recommendations were not applied.

The first recommendation would be to optimize the contact with the new evaporation mask. Either by abrading it between each use or cover the copper contacts with gold to prevent oxidation. Another option is to make larger copper contacts that would be easier to press on the gold contacts. These different solutions could not be tried due to lack of time.

Another recommendation would be to make a record of thickness versus conductivity as for samples HT, RT and LT, but before removing the samples from the evaporation chamber, to make a temperature ramp on them. This would enable to compute for the same sample, its bandgap by either the temperature ramp fitting or by the thickness dependence fitting and to see if both methods will give similar results.

This methodology was not applied for several reasons. The first being that the first evaporation mask required a day for bounding. Therefore, the priority was to make several observations on a single sample in order to spare time. With the second mask, it was easier to change samples and the focused switched to obtain as much observations of this thickness dependence of conductivity as possible. This procedure neglected the temperature dependence aspect. A temperature dependence observation after the thickness dependence would spare time and make the results easier to compare

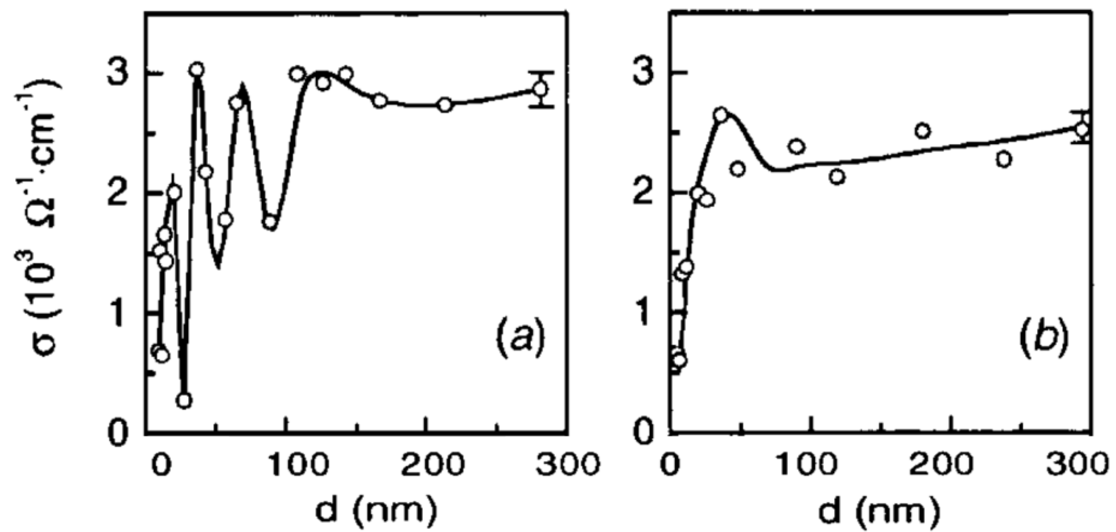

Figure 62: Conductivity as a function of the thickness. Results obtained by Rogacheva et al [21]. The samples were bismuth films deposited by thermal evaporation on mica substrate at a rate between 1 and 3 Å/s. The sample a) was deposited at 380K and sample b) at 300 K.

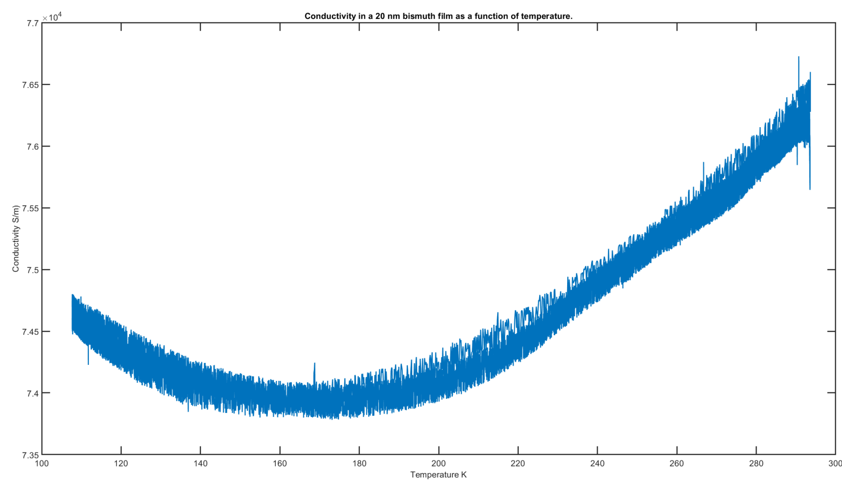

Figure 63: Conductivity as a function of temperature for 10nm sample with a conductivity valley. The minimum is for T=120K.

as both measurements would be carried on a single sample.

Question two and four concerning the oxidation of the film and the relaxation might be the questions where only a few more samples may be required to draw a significant conclusion. The other taking much more samples and time, it might be interesting to draw a conclusion for this part before focusing to the other questions.

Question six explain that data treatment of ex situ samples included several problems and challenges. Unfortunately these new data were provided only two weeks before the deadline. With a bit more time, some of the problems might have been solved and alternative to the initial experimental plan could be investigated.

Conclusions

This thesis investigated bismuth thin films deposited on a 90nm SiO_2 layer on top of Si(100). In order to carry out experiments, a setup was installed and an acquisition program was coded with Labview 2017 software, a new deposition mask was designed.

Several questions were to be raised. The objective of the thesis was to answer them as much as possible.

The first one is to determine if a significant difference is noticed between in situ and ex situ measurements. Without having enough samples to compare both, the outcome is that no meaningful difference is noticed.

The second one is to observe the impact of oxidation on the film. Only one sample was oxidized but a clear decrease in conductivity was observed. Extrapolation to determine the oxidation rate obtained give a similar result than literature. A fitting was to compare literature and our sample. Additional samples will check if the hypotheses are correct and will improve the fitting.

The third question is to check the influence of temperature deposition and thickness on conductivity. XRD measurements proves a difference in the crystalline structure between samples deposited at low temperature (110K) compared to samples deposited at room or high temperature (360K). Samples deposited at higher temperature exhibited higher conductivity. This is explained by larger grains present in these films. Literature tells us that for temperature approaching 200°C, the conductivity drops due to microstructure changes.

The fourth question is to quantify the impact of the film relaxation on its conductivity. It was found that the impact was of only [2-4%] after 16 h of relaxation. To reach a value of 15%, it would require more than one thousand hours of relaxation if the trends followed our higher bound fitting.

The fifth question concerns the oscillation of conductivity as a function of thickness. Oscillations were noted and vaguely corresponded to results that Rogacheva et al [21] obtained for deposition at room temperature. However we remain doubtful concerning the results for high deposition temperature (380K), especially for their fitting, as we did not observe similar behaviour on our samples.

The sixth and last question is to check if valleys of conductivity were present in our samples. This valleys were spot on several samples. The fact that they did not appear on all samples is probably because some samples could not be exposed to a temperature low enough. In addition to this, difficulties with data treatment prevented us to clearly observe this behaviour for low deposition temperature.

We provided an answer or some hypothesis for five of the six formulated questions. However these answers are often extrapolations due to limited amount of samples. We are conscious that the hypotheses could be wrong and that more samples are needed to confirm these trends. We provided a section with advises for the next persons who will carry on the project and hope that with more samples they will confirm or infirm those hypotheses.

Annexes

7.1 Two band model details

From [34], The induced current from an electric field perpendicular to a uniform magnetic field can be expressed as:

$$\mathbf{E} = \boldsymbol{\rho} \cdot \mathbf{j} \tag{14}$$

with the resistivity tensor being:

$$\boldsymbol{\rho} = \begin{bmatrix} \rho & -RH \\ RH & \rho \end{bmatrix}$$

considering a metal with n independent bands. Each having an induced current related to the magnetic field as $\mathbf{E_N} = \boldsymbol{\rho}_n \cdot \mathbf{j_n}$ and $\boldsymbol{\rho} = (\sum \boldsymbol{\rho}_n^{-1})^{-1}$ with $\boldsymbol{\rho}_n$:

$$\boldsymbol{\rho}_n = \begin{bmatrix} \rho_n & -R_n H \\ R_n H & \rho_n \end{bmatrix}$$

$$\boldsymbol{\rho}_n^{-1} = \frac{1}{\rho^2 + R^2 H^2} \begin{bmatrix} \rho & RH \\ -RH & \rho \end{bmatrix}$$

therefore:

$$\frac{1}{\rho^2 + R^2 H^2} \begin{bmatrix} \rho & RH \\ -RH & \rho \end{bmatrix} = \frac{1}{\rho_1^2 + R_1^2 H^2} \begin{bmatrix} \rho_1 & R_1 H \\ -R_1 H & \rho_1 \end{bmatrix} + \frac{1}{\rho_2^2 + R_2^2 H^2} \begin{bmatrix} \rho_2 & R_2 H \\ -R_2 H & \rho_2 \end{bmatrix}$$

$$\frac{\rho}{\rho^2 + R^2 H^2} = \frac{\rho_1}{\rho_1^2 + R_1^2 H^2} + \frac{\rho_2}{\rho_2^2 + R_2^2 H^2}$$

$$\frac{R}{\rho^2 + R^2 H^2} = \frac{R_1}{\rho_1^2 + R_1^2 H^2} + \frac{R_2}{\rho_2^2 + R_2^2 H^2}$$

using complex arithmetic:

$$\frac{\rho - iRH}{\rho^2 + R^2 H^2} = \frac{\rho_1 - iR_1 H}{\rho_1^2 + R_1^2 H^2} + \frac{\rho_2 - R_2 H}{\rho_2^2 + R_2^2 H^2}$$

by rearranging the terms:

$$\rho + iRH = \frac{(\rho_1 + iR_1H) \cdot (\rho_2 + iR_2H) \cdot (\rho_1 + \rho_2 - iH(R_1 + R_2))}{(\rho_1 + \rho_2)^2 + H^2(R1 + R_2)^2}$$

finally developing the numerator and taking respectively the real and imaginary part gives:

$$\rho_{Hall} = \frac{R_1R_2(R_1 + R_2)B^3 + (R_1\rho_2^2 + R_2\rho_1^2)B}{(\rho_1 + \rho_2)^2 + (R_2 + R_1)^2B^2} \tag{15}$$

$$\rho = \frac{\rho_1\rho_2(\rho_1 + \rho_2) + (\rho_1R_2^2 + \rho_2R_1^2)B^2}{(\rho_1 + \rho_2)^2 + (R_1 + R_2)^2B^2} \tag{16}$$

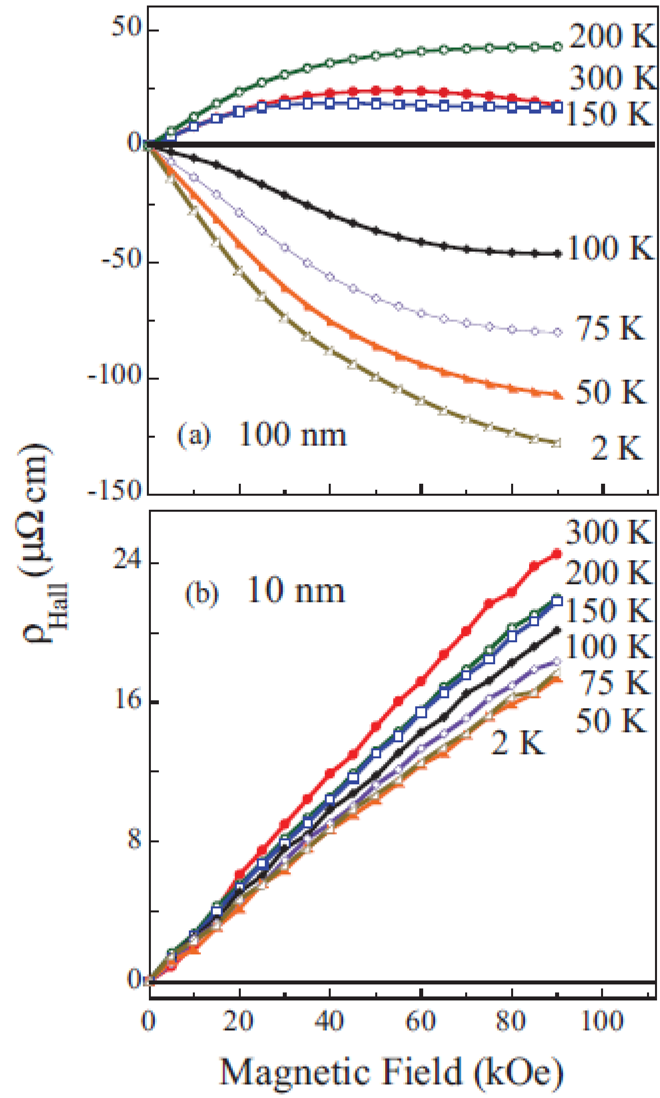

Figure 64: (Colour online) Corrected Hall resistivity $_{Hallisotherms}$ at selected temperatures in the 2 to 300 K range for the sake of clarity as a function of magnetic field for (a) t = 100 nm and (b) t = 10 nm thick Bi films as representative samples of the present study. Solid lines drawn are guides to the eye[22].

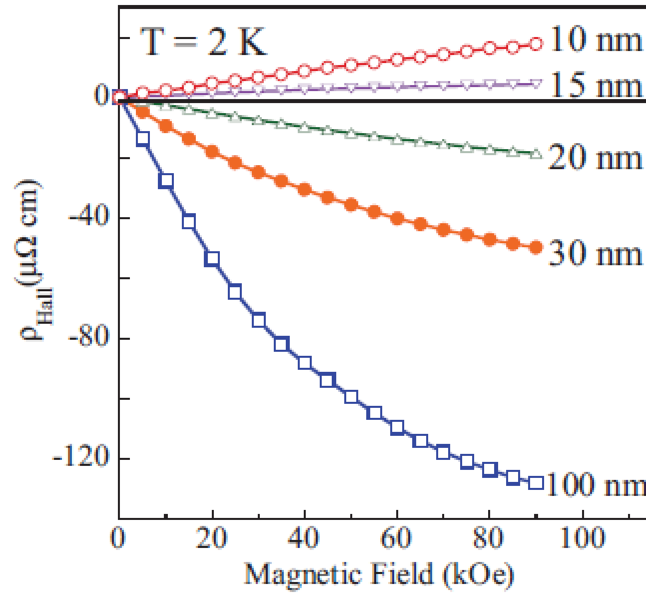

Figure 65: (Colour online) Corrected Hall resistivity Hall as a function of magnetic field for several film thicknesses in the 10 to 100 nm range as representative of this study at 2 K. Solid lines drawn are guides to the eye.[22].

References

[1] L. Kumari, S.-J. Lin, J.-H. Lin, Y.-R. Ma, P.-C. Lee, and Y. Liou, "Effects of deposition temperature and thickness on the structural properties of thermal evaporated bismuth thin films," *Applied Surface Science*, vol. 253, no. 14, pp. 5931–5938, 2007.

[2] W. M. Haynes, *CRC handbook of chemistry and physics.* CRC press, 2014.

[3] S. Condurache-Bota, R. DRAȘOVEAN, N. ȚIGĂU, and A. P. Rambu, "The influence of substrate temperature on the structure and on the optical reflection spectrum of bismuth thin films," *Rev. Roum. Chim*, vol. 56, no. 12, pp. 1101–1106, 2011.

[4] C. Hoffman, J. Meyer, F. Bartoli, A. Di Venere, X. Yi, C. Hou, H. Wang, J. Ketterson, and G. Wong, "Semimetal-to-semiconductor transition in bismuth thin films," *Physical Review B*, vol. 48, no. 15, p. 11431, 1993.

[5] T. N. Bui, J.-P. Raskin, and B. Hackens, "Semiconductor-to metallic-like behavior in bi thin films on kcl substrate," *Journal of Applied Physics*, vol. 119, no. 13, p. 135304, 2016.

[6] J. L. Yarnell, J. L. Warren, R. G. Wenzel, and S. H. Koenig, "Phonon dispersion curves in bismuth," *IBM Journal of Research and Development*, vol. 8, no. 3, pp. 234–240, 1964.

[7] E. Murray, S. Fahy, D. Prendergast, T. Ogitsu, D. Fritz, and D. Reis, "Phonon dispersion relations and softening in photoexcited bismuth from first principles," *Physical Review B*, vol. 75, no. 18, p. 184301, 2007.

Figure 66: Detailed schematic of the mask.

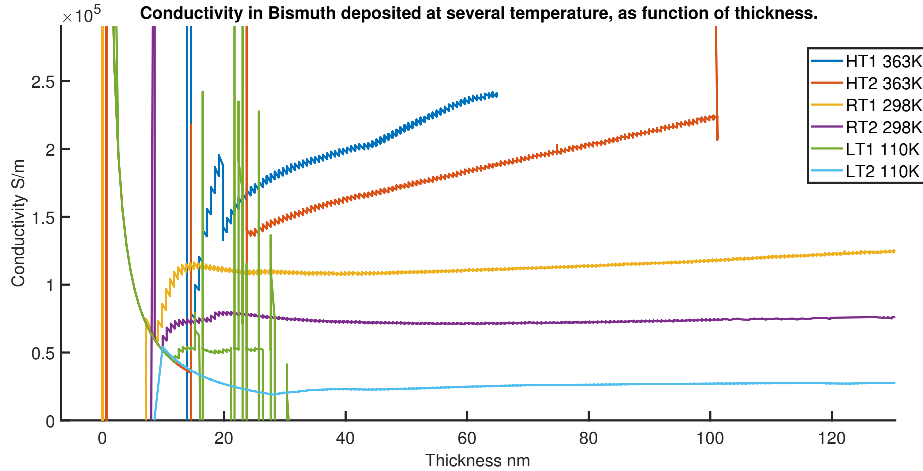

Figure 67: Conductivity as a function of the thickness for different deposition temperature. With sample LT1.

[8] B. Hackens, *Coherent and ballistic transport in InGaAs and Bi mesoscopic devices*. PhD thesis, PhD thesis, Université Catholique de Louvain, 2005.

[9] L. Díaz-Sánchez, A. Romero, and X. Gonze, "Phonon band structure and interatomic force constants for bismuth: Crucial role of spin-orbit interaction," *Physical Review B*, vol. 76, no. 10, p. 104302, 2007.

[10] M. Aitani, T. Hirahara, S. Ichinokura, M. Hanaduka, D. Shin, and S. Hasegawa, "In situ magnetotransport measurements in ultrathin bi films: evidence for surface-bulk coherent transport," *Physical review letters*, vol. 113, no. 20, p. 206802, 2014.

[11] A. Van der Drift, "Evolutionary selection, a principle governing growth orientation in vapour-deposited layers," *Philips Res. Rep*, vol. 22, no. 3, p. 267, 1967.

[12] H.-H. Sun, M.-X. Wang, F. Zhu, G.-Y. Wang, H.-Y. Ma, Z.-A. Xu, Q. Liao, Y. Lu, C.-L. Gao, Y.-Y. Li, *et al.*, "Coexistence of topological edge state and superconductivity in bismuth ultrathin film," *Nano Letters*, vol. 17, no. 5, pp. 3035–3039, 2017.

[13] Y. Ahn, Y.-H. Kim, S.-I. Kim, and K.-H. Jeong, "Thickness dependent surface microstructure evolution of bismuth thin film prepared by molecular beam deposition method," *Current Applied Physics*, vol. 12, no. 6, pp. 1518–1522, 2012.

[14] S. Rodil, O. Garcia-Zarco, E. Camps, H. Estrada, M. Lejeune, L. Bourja, and A. Zeinert, "Preferential orientation in bismuth thin films as a function of growth conditions," *Thin Solid Films*, vol. 636, pp. 384–391, 2017.

[15] S. Middleman and A. K. Hochberg, *Process engineering analysis in semiconductor device fabrication*. Mcgraw-Hill College, 1993.

[16] Y. Liu and R. E. Allen, "Electronic structure of the semimetals bi and sb," *Physical Review B*, vol. 52, no. 3, p. 1566, 1995.

[17] N. Marcano, S. Sangiao, C. Magén, L. Morellón, M. Ibarra, M. Plaza, L. Pérez, and J. De Teresa, "Role of the surface states in the magnetotransport properties of ultrathin bismuth films," *Physical Review B*, vol. 82, no. 12, p. 125326, 2010.

[18] D. Lükermann, S. Sologub, H. Pfnür, and C. Tegenkamp, "Sensing surface states of bi films by magnetotransport," *Physical Review B*, vol. 83, no. 24, p. 245425, 2011.

[19] S. Xiao, D. Wei, and X. Jin, "Bi (111) thin film with insulating interior but metallic surfaces," *Physical review letters*, vol. 109, no. 16, p. 166805, 2012.

[20] N. Marcano, S. Sangiao, J. De Teresa, L. Morellón, M. Ibarra, M. Plaza, and L. Pérez, "Structural and magnetotransport properties of bi thin films grown by thermal evaporation," *Journal of Magnetism and Magnetic Materials*, vol. 322, no. 9, pp. 1460–1463, 2010.

[21] E. Rogacheva, S. Grigorov, O. Nashchekina, S. Lyubchenko, and M. Dresselhaus, "Quantum-size effects in n-type bismuth thin films," *Applied physics letters*, vol. 82, no. 16, pp. 2628–2630, 2003.

[22] N. Marcano, S. Sangiao, C. Magén, L. Morellón, M. Ibarra, M. Plaza, L. Pérez, and J. De Teresa, "Erratum: Role of the surface states in the magnetotransport properties of ultrathin bismuth films [phys. rev. b 82, 125326 (2010)]," *Physical Review B*, vol. 87, no. 19, p. 199904, 2013.

[23] R. Hartman, "Temperature dependence of the low-field galvanomagnetic coefficients of bismuth," *Physical Review*, vol. 181, no. 3, p. 1070, 1969.

[24] R. A. Hoffman and D. Frankl, "Electrical transport properties of thin bismuth films," *Physical Review B*, vol. 3, no. 6, p. 1825, 1971.

[25] C. Yang, "A study of electrical properties in bismuth thin films," *University of Florida. Gainesville*, p. 18, 2008.

[26] H. Chu, P. Henriksen, and J. Alexander, "Resistivity and transverse magnetoresistance in ultrathin films of pure bismuth," *Physical Review B*, vol. 37, no. 8, p. 3900, 1988.

[27] S. Cho, Y. Kim, A. Freeman, G. Wong, J. Ketterson, L. Olafsen, I. Vurgaftman, J. Meyer, and C. Hoffman, "Large magnetoresistance in postannealed bi thin films," *Applied Physics Letters*, vol. 79, no. 22, pp. 3651–3653, 2001.

[28] R. Koseva, I. Mönch, D. Meier, J. Schumann, K.-F. Arndt, L. Schultz, B. Zhao, and O. Schmidt, "Evolution of hillocks in bi thin films and their removal upon nanoscale mechanical polishing," *Thin Solid Films*, vol. 520, no. 17, pp. 5589–5592, 2012.

[29] A. Ramadan, A. El-Shabiny, and N. El-Sayed, "Size-dependent structural characteristics of thin bismuth films," *Thin Solid Films*, vol. 209, no. 1, pp. 32–37, 1992.

[30] P. M. v. A. W. J. de Haas *Leiden Commun*, p. No. 108d, 1930.

[31] Z. Zhang, X. Sun, M. Dresselhaus, J. Y. Ying, and J. Heremans, "Electronic transport properties of single-crystal bismuth nanowire arrays," *Physical Review B*, vol. 61, no. 7, p. 4850, 2000.

[32] P. Kröger, D. Abdelbarey, M. Siemens, D. Lükermann, S. Sologub, H. Pfnür, and C. Tegenkamp, "Controlling conductivity by quantum well states in ultrathin bi (111) films," *Physical Review B*, vol. 97, no. 4, p. 045403, 2018.

[33] R. Atkinson and E. Curran, “Ellipsometric examination of the oxidation of vacuum-deposited bismuth films,” *Thin solid films*, vol. 128, no. 3-4, pp. 333–339, 1985.

[34] N. W. Ashcroft, N. D. Mermin, and S. Rodriguez, “Solid state physics,” 1978.

Rue Archimède, 1 bte L6.11.01, 1348 Louvain-la-Neuve **www.uclouvain.be/epl**